

Stathmin-tubulin interaction gradients in
motile and mitotic *Xenopus laevis* cells

Dissertation

zur Erlangung des Doktorgrades des Fachbereiches
Biologie der
Universität Hamburg

vorgelegt von
Philipp Niethammer
aus Heilbronn, Deutschland

Hamburg, 2005

Table of contents

Abstract	1
<hr/>	
I. Introduction	2
A. Microtubules: a versatile polymer at the origin of various cell shapes	3
B. Principles underlying cytoskeletal self-organization	5
B1. Dynamic Instability	5
B2. Search and capture	7
B3. Polarized growth	8
B4. Molecular motors	9
C. Signaling mechanisms involved in microtubule dynamics and organization	11
C1. Global regulation of microtubule dynamics by microtubule associated proteins (MAPs)	11
C2. Local regulation of microtubule dynamics	12
D. Fluorescence Resonance Energy Transfer (FRET) as a tool to assess local microtubule regulation	15
D1. Principle	15
D2. Intensity based FRET detection	16
E. The microtubule-destabilizing protein stathmin/op18	18
<hr/>	
II. Aim of the thesis	21
<hr/>	
III. Results	23
A. Detection of stathmin-tubulin interaction in vitro	24
A1. Two component system: GFP-stathmin and Rhodamine-tubulin	24
A2. One component system: COPY	28
A3. Summary	33
B. COPY detects phosphorylation dependent stathmin-tubulin interaction in <i>Xenopus</i> Egg extracts	35

C. Illuminating stathmin-tubulin interaction in cells	36
C1. Characterizing exogenous stathmin expression in cells	36
C2. Stathmin-tubulin interaction gradients in interphase cells	40
C3. Stathmin-tubulin interaction gradients in mitotic cells	46

IV. Discussion	49
A. Stathmin-tubulin interaction gradients in interphase	50
B. Stathmin-tubulin interaction gradients in mitosis	52
C. Conclusion	54

V. Materials and Methods	55
A. Materials	56
A1. Chemicals	56
A2. Commonly used buffers, solutions and media	56
A3. Instruments	59
A4. Kits	60
A5. Antibodies	60
A6. Bacterial strains	61
A7. Cell lines	62
A8. Plasmids	62
B. Common DNA methods	66
B1. Polymerase chain reaction (PCR)	66
B2. DNA electrophoresis	67
B3. DNA extraction from agarose gels	67
B4. Determination of DNA concentration and purity	67
B5. DNA digestion by restriction enzymes	68
B6. DNA ligation	68
B7. Transformation of competent bacteria	69
B8. Lipid mediated transfection of eukaryotic cells	69
B9. Transfection of eukaryotic cells by electroporation	70
C. Common biochemical methods	70
C1. Preparation of Xenopus egg extracts	70
C2. Rhodamine labeling of tubulin	71
C3. Expression and purification of recombinant stathmin	73

C4. <i>In vitro</i> phosphorylation of recombinant stathmin	74
C5. SDS-polyacrylamide gel electrophoresis (SDS-PAGE)	75
C6. Coomassie staining of gels	75
C7. Western blotting	76
D. Fluorescence based methods	76
D1. Wavelength spectrum of COPY	76
D2. Ratiometric analysis of COPY-tubulin interaction <i>in vitro</i>	77
D3. Ratiometric analysis of COPY-tubulin interaction in <i>Xenopus</i> egg extracts	78
D4. Determination of exogenous protein expression level in <i>Xenopus</i> cells	78
D5. Ratiometric analysis of COPY-tubulin interaction in <i>Xenopus</i> cells	78
D6. Acceptor photobleaching analysis of COPY-tubulin interaction in <i>Xenopus</i> cells	79
D7. Fluorescence recovery after photobleaching (FRAP)	80
E. Culture, drug treatment and immunostaining of cells	81
E1. Cell culture and freezing	81
E2. Drug treatment of cells	81
E3. Fixation and immunostaining of cells	82
F. Estimation of gradient extent	82
VI. References	85

Abbreviations	96
Curriculum vitae	97
Acknowledgements	99

Abstract

The spatial organization of the microtubule cytoskeleton is thought to be directed by steady-state activity gradients of diffusible regulatory molecules. Here we report the visualization of such intracellular gradients by monitoring the interaction between tubulin and a regulator of microtubule dynamics, stathmin, using a fluorescence resonance energy transfer (FRET) based biosensor. These gradients were observed both during interphase in lamella and during mitosis around chromosomes suggesting that formally similar mechanisms contribute to the creation of polarized microtubule structures. We provide evidence that the stathmin-tubulin interaction patterns reflect steady-state gradients of stathmin phosphorylation in these areas.

I. Introduction

A. Microtubules: a versatile polymer at the origin of various cell shapes

Cells diverge into a variety of different forms, supporting a particular function within a tissue or organism (Figure 1). Since the cytoplasm and the plasma membrane are rather fluid, they cannot serve to maintain a certain cell shape.

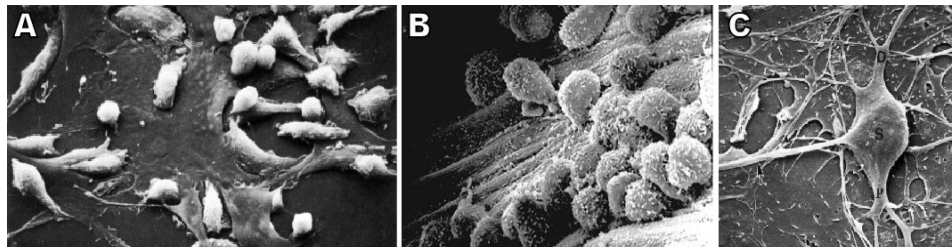


Figure 1. Electron micrographs of different types of animal cells. **(A)** Fibroblasts. **(B)** White blood cells. **(C)** Neurons.

Thus, especially in animal cells, which miss a rigid cell wall, a cytoskeleton is needed to provide mechanical stability. In addition to actin- and intermediate filaments, microtubules are one of the three major building polymers of the cellular cytoskeleton. Microtubules are long, hollow cylinders with an outer diameter of 25 nm formed by the lateral interaction of protofilaments.

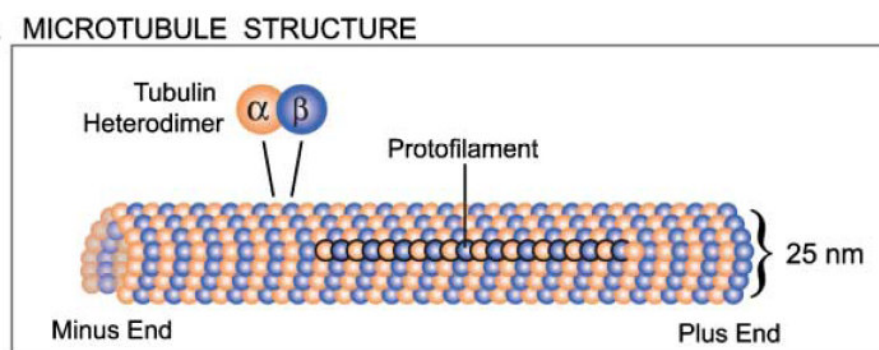


Figure 2. Schematic view of microtubule structure (adapted from Kline-Smith&Walczak, 2004).

These are linear polymers of tubulin heterodimers which associate longitudinally by head to tail interaction in a GTP dependent manner (Figure 2).

Similar to the other cytoskeletal components, microtubules serve to spatially organize the cytoplasm: They connect protein complexes and organelles from different regions of the cell and provide tracks for transport between them. Moreover, they increase the mechanical stability of the cell and thereby help to preserve distinct cell shapes.

The arrangement of the microtubule array can vary largely among cells. It is always tailored to a specific cell-type, cell cycle-stage or differentiation-stage specific function.

This diversity impressively demonstrates, how individually microtubules are able to selforganize under altered cell type-, cycle-, or differentiation-stage specific molecular regimes. Within the same organism these different regimes are generated by transcriptional and/or posttranslational derivation of one genetic repertoire. This raises the question, what the driving forces of cytoskeletal selforganization are.

B. Principles underlying cytoskeletal self-organization

Any assembly of resources and procedures united and regulated by interaction or interdependence to accomplish a set of specific functions can be termed *system*. The process of functional assembly within a system is by definition a *selforganization* process.

Concerning cytoskeletal morphogenesis, the system of interest is the assembly of all molecules and “procedures” needed to build a spindle, or an interphase cytoskeleton. Some mechanistical descriptions of these “procedures” were proposed as follows.

B1. Dynamic instability

Microtubules frequently switch between periods of growth and shrinking. This *dynamic instable* (Mitchison and Kirschner 1984) behavior is thought to be a consequence of the delayed hydrolysis of GTP after tubulin assembly. If tubulin is added to a microtubule tip faster than the GTP, which it carries, can be hydrolyzed, a “GTP cap” forms on the end of the polymer, which promotes further tubulin addition. This is due to the fact that tubulin molecules carrying GTP interact with higher affinity than tubulin molecules loaded with GDP. Conversely, if the rate of polymerization slows down, the microtubule end will lose its GTP cap because the rate of nucleotide hydrolysis exceeds the rate of subunit addition. The microtubule will start and continue to shrink (Figure 3).

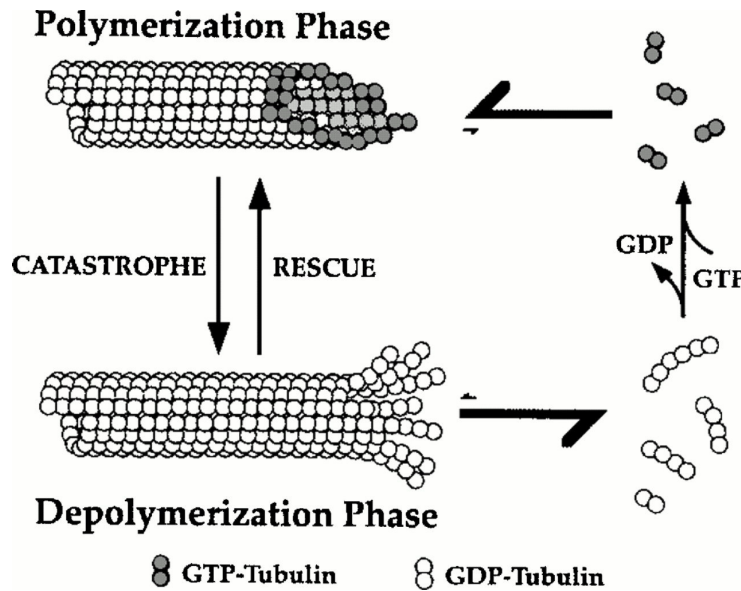


Figure 3. (adapted from Desai & Mitchison, 1997) Microtubule (MT) dynamic instability. GTP-tubulin is incorporated at polymerizing MT ends, the bound GTP is hydrolyzed during or soon after polymerization, and Pi is subsequently released. Thus the MT lattice is predominantly composed of GDP-tubulin (and is often referred to as a GDP MT in the text). Polymerizing MTs infrequently transit to the depolymerization phase (catastrophe). Depolymerization is characterized by the very rapid loss of GDP-tubulin subunits and oligomers from the MT end. Depolymerizing MTs can also infrequently transit back to the polymerization phase (rescue). The transitions in dynamic instability are measured as frequencies (e.g. catastrophe frequency = number of catastrophes per unit time in the polymerization phase). The term frequency is used rather than rate because it is not clear if the transitions are simple first order processes. This representation incorporates the notions of a small GTP/GDP-Pi cap acting as a stabilizing structure at polymerizing ends and different conformational configurations at polymerizing and depolymerizing ends. For quantitative details on the various parameters, see Walker et al (1988) (adapted from Inoué & Salmon 1995).

Microtubule dynamic instability is defined by four parameters that can be measured by video microscopy: the growth rate (V_g), the shrinking rate (V_s), the catastrophe rate (transition from growth to shrinkage or f_{cat}), and the rescue rate (transition from shrinkage to growth or f_{res}). These parameters can be independently regulated by microtubule associated proteins (MAPs) or other regulatory factors. Thus, dynamic instability makes microtubule growth susceptible to its molecular environment.

B2. Search and capture

Due to dynamic instability the microtubule array in a cell constantly turns over. Microtubules shrink and disappear while new ones grow out from the centrosome.

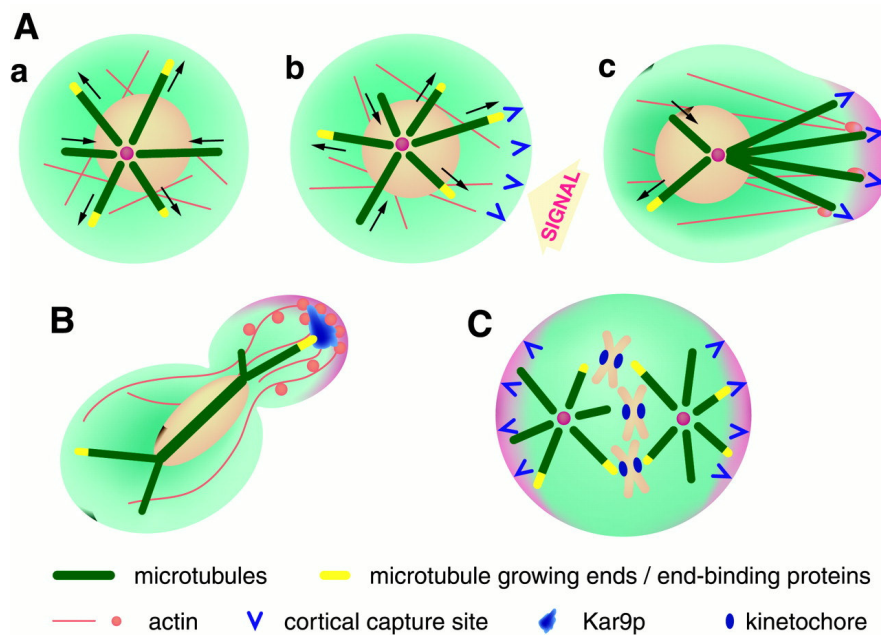


Figure 4. (adapted from Mimori-Kiyosue & Tsukita, 2001). Microtubules and search-and-capture. **(A)** The microtubule search-and-capture mechanism, modified from Kirschner and Mitchison (1986). (a) In unpolarized cells, microtubules interconvert between growing and shortening with no preferred direction by dynamic instability, which enables microtubules to explore all over the cellular space. The growing microtubule ends are always capped by microtubule end binding proteins such as EB1. (b) A local spatial cue activates some microtubule-capturing sites at the cell cortex. (c) Some microtubules are captured and selectively stabilized, which induces asymmetric orientation of the microtubule-based cytoskeleton. **(B)** In the budding yeast, the spindle microtubules originating from the spindle pole body on the nuclear envelope search for and capture the tips of daughter buds. **(C)** Microtubule search-and-capture mechanism during mitosis of higher organisms. Microtubules search for the kinetochores or attachment sites on the cortex to capture the chromosomes or to orient spindle microtubules, respectively.

Some microtubules become stabilized or capped by molecular factors located on specific structures or in particular regions of the cell (e.g. cell cortex) preventing or decreasing their disassembly.

The number of these less dynamic polymers of particular directionality accumulates over time resulting in a net-polarized array. Since the microtubule ends constantly probe the cytoplasm around them before they finally get stabilized on a structure, this behavior is termed *search and capture* (Figure 4). It becomes especially apparent during cell division, where the chromosome kinetochores capture the ends of the spindle microtubules.

B3. Polarized growth

A polarized microtubule array can be observed in very dynamic processes like cell migration or division. When cells move, the microtubules have to invade the space captured by the protruding lamella. Although the polymers branch out in all directions from the centrosome, the number of microtubules extending in the direction of movement predominates. Similar, during mitosis, microtubule growth is focused on the chromosomes.

It is not really clear how this selectivity in growth is achieved. *Dynamic instability* seems to be a basic requirement for this behavior but *search and capture* alone cannot fully explain it since polarization by *search and capture* is a direct consequence of microtubule immobilization (“capture”) and the resulting structure therefore should be rather static.

However, experimental observations indicate that this is not the case. Both, the mitotic spindle and the microtubule cytoskeleton of a moving cell are polarized and at the same time dynamic structures. This can be explained by assuming that the process of microtubule growth itself is polarized or directionally biased. Evidence for this is accumulating: In mitotic *Xenopus* egg extracts, for example, aster anisotropy has been found to be biased into the direction of the chromatin and the catastrophe frequency reduced in its vicinity (Dogterom, Felix et al. 1996; Carazo-Salas

and Karsenti 2003). In addition, simulation of kinetochore positioning in yeast (Sprague, Pearson et al. 2003) as well as prediction of prometaphase duration in mammalian cells by mathematical modeling (Wollmann, Cytrynbaum et al. 2004, personal communication) only fit to the real observations if it is assumed that microtubule growth is biased by chromosomes.

B4. Molecular motors

Polarized arrays of microtubules can also be created by reorganization of preexisting microtubules in the absence of nucleating centers.

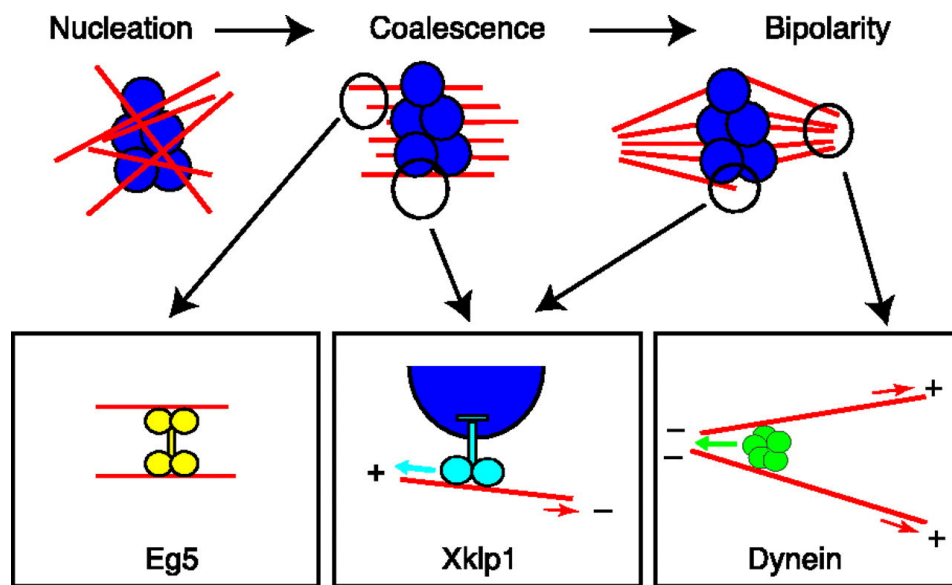


Figure 5. (adapted from Karsenti & Vernos, 2001) Role of motors in spindle self-organization. Randomly nucleated microtubules become aligned by a cross-linking motor (Eg5). The chromosome-associated plus end-directed motor Xklp1 captures microtubules on the chromatin and pushes their minus ends away, leading to their sorting into two half-spindles on each side of the chromosome mass. Then, a multimeric form of the minus-end motor dynein focuses spindle poles. This is an intuitive working model based on many experiments carried out in egg extracts. But it probably reflects, to some extent, the principles involved in spindle assembly and stability. Red arrows indicate the direction of movement of a microtubule; arrows in the same color as a motor indicate the direction of movement of the motor.

Two types of molecular motors drive this process: dynein-like proteins, which move toward the minus end and kinesin-like proteins that move toward the plus end. By cross linking and concomitant movement on the microtubules, these motors can exert structuring forces that reorganize the array in a way that is mainly dependent on the biochemical and physical properties of the motor (Surrey, Nedelec et al. 2001). The integrity of microtubule array morphology is dependent on the proper function of these motors. Interference with this function causes severe defects in microtubule array assembly e.g. serious spindle defects (Goshima and Vale 2003).

C. Signaling mechanisms involved in microtubule dynamics and organization

C1. Global regulation of microtubule dynamics by microtubule associated proteins (MAPs)

Microtubule growth *in vivo* is altered by a variety of regulatory proteins (Figure 6C). These proteins can either promote or inhibit polymer growth by changing the parameters of dynamic instability (V_g , V_s , f_{cat} , f_{res}).

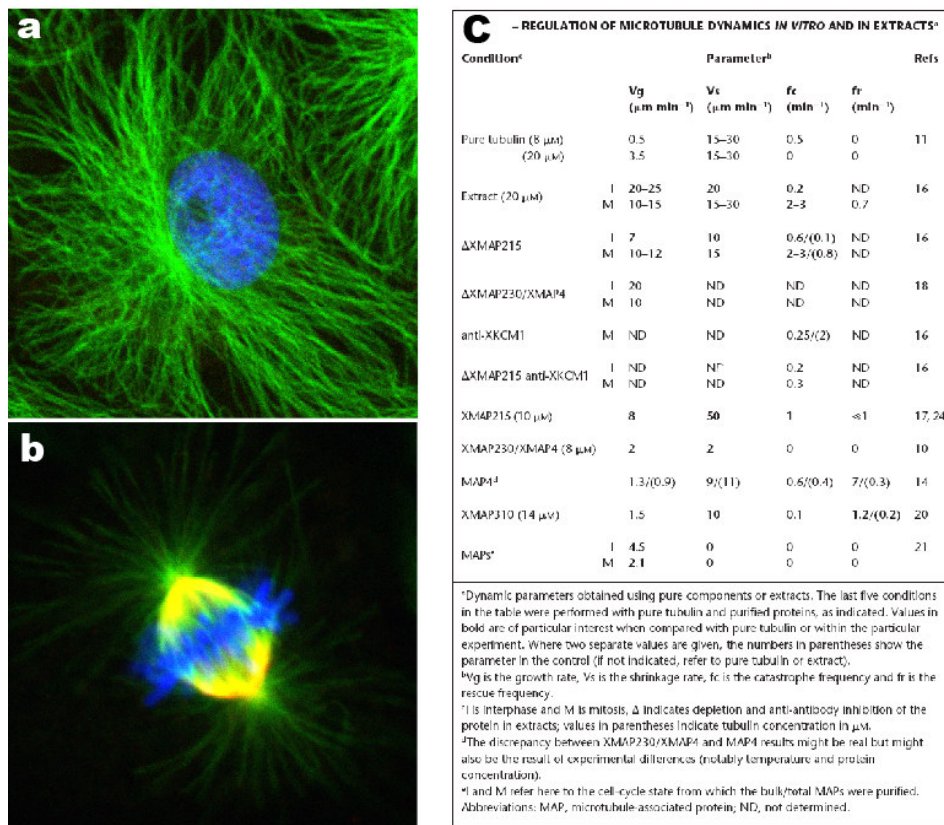


Figure 6. The morphological difference of the microtubule cytoskeleton in (A) interphase and versus (B) mitosis is correlated with (C) different parameters of dynamic instability in both states. Various MAPs regulate these parameters. Depletion of these proteins from *Xenopus* Egg Extracts reveals their regulative contribution to microtubule dynamics in both stages of the cell cycle (table adapted from Andersen, 2000).

Global regulation of these components on the transcriptional or post-translational level is utilized by the cell to change the general dynamic properties of a microtubule array (Figure 6A, B). This happens for example at the transition from interphase to mitosis. The microtubules of an interphase array are longer than mitotic ones because in interphase microtubules undergo catastrophes with a roughly tenfold lower frequency than in mitosis.

This cell cycle dependent change in dynamics is due to posttranslational modification of MAP activity initialized by the activity of cyclin dependent kinase 2 (cdc2).

Two general mechanisms for the action of microtubule regulators are plausible: They can either act on the tubulin subunit level, promoting or hindering assembly into polymers, or they interact with pre-assembled microtubules, inducing or preventing catastrophes. Stathmin/op18 is an example for a microtubule regulator that acts on the tubulin subunit level. Other MAPs like EB1, CLIP170 or APC can be observed at microtubule tips and are therefore supposed to modulate polymer stability by altering tip integrity. An interesting feature of most of these proteins is that their activity in a complex system, e.g. a cell or egg extract, cannot be reconstituted *in vitro*. This indicates that they need additional factors to support their *in vivo* function.

C2. Local regulation of microtubule dynamics

Polarized growth has been explained by the hypothetical existence of steady-state gradients of microtubule regulating activities, such as a gradient of Ran-GTP (Carazo-Salas, Guarguaglini et al. 1999; Kalab, Pu et al. 1999)(Figure 7B). In the vicinity of mitotic chromatin the small GTPase Ran is continuously reloaded with GTP due to the action of the nucleotide exchange factor (GEF) RCC1, which is localized on chromosomes. In conjunction with the counteracting activity of the cytoplasmic GTPase activating protein Ran-GAP that inactivates Ran, a steady-state gradient of GTPase activity is created. It was directly visualized using biosensors

based on fluorescence energy transfer (FRET) (Kalab, Weis et al. 2002). Rather than being a direct regulator of microtubule growth, the Ran gradient seems to be a spatially regulated “master switch” of chromosome-biased downstream processes like TPX2 mediated microtubule nucleation (Gruss, Carazo-Salas et al. 2001; Schatz, Santarella et al. 2003) and probably also stabilization. In addition to the Ran gradient, a graduated activity of the microtubule destabilizing protein stathmin/op18 has been hypothesized to exist around mitotic chromatin (Andersen, Ashford et al. 1997) established by the counterplay of chromatin localized kinases such as Polokinese 1 (Budde, Kumagai et al. 2001) and soluble cytoplasmic phosphatase like PP2A (Figure 7A).

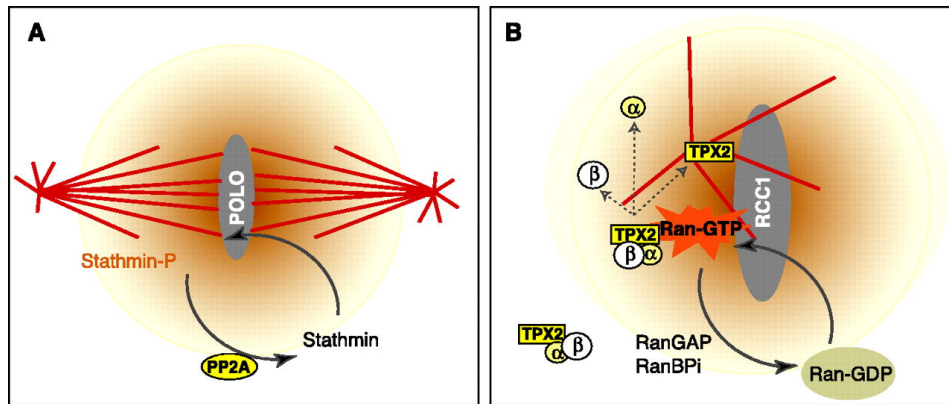


Figure 7. (adapted from Karsenti & Vernos, 2001) **(A)** A hypothetical phosphorylation gradient of the microtubule-destabilizing factor stathmin. A chromosomal kinase (polo) would locally phosphorylate stathmin, which is kept in a dephosphorylated state by a type 2A phosphatase in the cytoplasm. The relative kinetics of phosphorylation, dephosphorylation, and diffusion of stathmin would result in a gradient of stathmin phosphorylation. Because stathmin destabilizes microtubules when not phosphorylated, this could result in local microtubule stabilization around chromosomes. **(B)** A hypothetical Ran-GTP gradient around chromosomes. Ran is kept in a GDP form in the cytoplasm by a soluble Ran GTPase-activating enzyme (RanGAP) and loaded with GTP by the RCC1 GEF factor concentrated on chromosomes, resulting in a steady-state Ran-GTP gradient. The presence of Ran-GTP around chromosomes dissociates a complex made of importins (alpha, beta) and TPX2. When released from the complex, TPX2 nucleates microtubules. The Ran gradient has other effects, such as stabilizing microtubules and activating motors.

Such a gradient would have the potential to bias microtubule growth by lowering the catastrophe frequency of microtubules approaching the chromosomes and increasing the chance of catastrophe for microtubules that branch into other directions. However, spatial regulation of stathmin has never been shown yet.

There are also indications for biased microtubule growth in interphase cells: During migration, microtubule plus ends are often found close to the leading edge. Since this is constantly pushing forward, the microtubules have to undergo net-growth. Indeed, near the leading edge a subset of microtubules spends more time in growing than the microtubules in the other parts of the cell (Wittmann and Waterman-Storer 2001). This biased behavior has been termed "pioneering" and it seems to depend on the action of the small GTPase Rac1 and its downstream effectors including Pak1 (Wittmann, Bokoch et al. 2003; Wittmann, Bokoch et al. 2004) and others. Interestingly, a gradient of Rac1 activity has been visualized by FRET based techniques to decay from the leading edge to the rear of the cell. It correlates with the direction of movement (Kraynov, Chamberlain et al. 2000). Similarly, in a wound-healing assay active Pak1 localizes preferentially to the leading edges of migrating cells (Sells, Pfaff et al. 2000). It appears that the direction of net-growth correlates with the spatial bias of biochemical activity that mediates this growth. One protein that is suspected to translate the spatially biased activity of the Rac1-Pak1 pathway into directional microtubule growth is stathmin/op18. A small fraction of this protein has been shown to be phosphorylated and inactivated by this signaling cascade (Daub, Gevaert et al. 2001). This corresponds well to the idea that stathmin/op18 could be inactivated locally at the leading edge. However, this has never been demonstrated directly.

D. Fluorescence Resonance Energy Transfer (FRET) as a tool to assess local microtubule regulation

D1. Principle

In order to assess the local regulatory activities in cells, methods are required that can detect protein-protein interactions with spatial resolution. The discovery of the green fluorescent protein (GFP) technology has opened up ways to achieve this.

Light emission by a fluorophore is sensitive to its molecular environment and thus can be utilized to gather information about the system the fluorophore was introduced to. The fluorophore emission can be monitored with the help of optical devices, such as microscopes or fluorimeters, without disturbing the system.

Changes in the molecular conformation of a fluorophore are likely to alter their ability to emit fluorescence light. These changes can be induced by a change in e.g. the ionic environment of the fluorophore but also by direct physical interaction with other molecules. By chemical or genetic engineering, fluorophores can be brought into such a molecular context that a specific molecular interaction will affect their structure and thus their fluorescence properties.

In addition, changes in fluorescence properties of a fluorophore can also be induced without affecting its molecular structure. Close proximity of two fluorophores for example, can give rise to a physical phenomenon that affects the fluorescence properties of both: FRET is a process in which a *donor*-fluorophore in the excited state transfers energy via dipole-dipole coupling to an acceptor in close proximity (< 8 nm) and proper relative angular orientation (Förster 1948; Herman 1989). Occurrence of FRET results on the one hand in quenching of the donor emission and increased (“sensitized”) acceptor emission. Since the efficiency

of energy transfer is inversely proportional to the sixth power of the distance between donor and acceptor (Figure 8B), FRET can be used to probe in real-time whether two proteins interact or not (Miyawaki 2003).

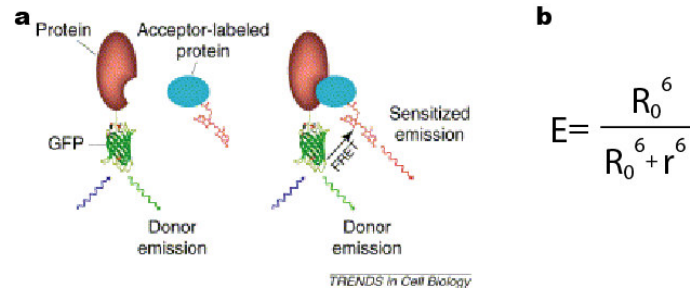


Figure 8. (A) (adapted from Wouters et al., 2001) Schematic representation of two component FRET. **(B)** The FRET-efficiency (E) increases with decreasing distance (r) between the two fluorophores. R_0 is the distance at which 50% energy transfer takes place (typically 2-6 nm).

There are two different types of approaches, how FRET can be used to assess protein-protein interaction: In general, both putative interaction partners can be chemically or genetically labeled with different fluorophores. With this approach bimolecular interactions can be specifically detected (Figure 8A). In particular cases, the interaction induces a conformational change within one or both of the binding partners. This property can be utilized to construct “one component” FRET sensors, where both different fluorophores are present within the same molecule. In case of an interaction, the two fluorophores are brought in proximity or separated by the intramolecular conformational change inducing an increase or decrease of FRET, respectively.

D2. Intensity based FRET detection

In intensity based methods the change in the ratio of the donor and acceptor emissions upon occurrence of FRET is determined. Despite its practicality, this measurement suffers from various drawbacks. Since fluo-

rescence intensity is proportional to fluorophore concentration, the donor/acceptor intensity ratio will depend on local concentrations of labelled proteins. Differential distribution of the fluorescent proteins, a result of biological activity during the measurement, makes this aspect particularly problematic. In addition, due to the partial spectral overlap of donor and acceptor fluorophores, corrections are necessary for donor bleed-through into the acceptor detection channel and for direct excitation of the acceptor. These involve the acquisition of images of three samples containing the donor, the acceptor and both donor/acceptor, the use of three different filter settings and subsequent mathematical procedures (Gordon, Berry et al. 1998). Chromatic aberration, wrong pixel alignment and rapid organelle movements, e.g. membrane ruffling, can result in noise and/or artefacts when these image-processing algorithms are applied. Ratiometric concentration effects are not an issue if reporter probes are used which encode the donor and acceptor GFPs on the same polypeptide like the construct used for the present study. Here, the stoichiometry of the donor/acceptor is constant for all pixels and therefore any change in emission ratio can be ascribed to changes in FRET efficiency.

A simple and more reliable intensity-based method that does not require corrections for the acceptor fluorescence is the detection of dequenching of the donor fluorescence by acceptor photobleaching (Bastiaens et al., 1996). This method, however, is restricted to a single measurement and requires prolonged illumination during which relocation of the donor-tagged molecules could occur.

E. The microtubule destabilizing protein stathmin/op18

Stathmin/op18 is a 17 kD, cytoplasmic protein with microtubule destabilizing activity. It is expressed in all cell types with varying levels ranging from 0.005% to 0.5% (Brattsand, Roos et al. 1993). Highest levels are found in fast proliferating cells like cancer cells; lowest levels are present in terminally differentiated cells like neurons (Brattsand, Roos et al. 1993; Rowlands, Williams et al. 1995).

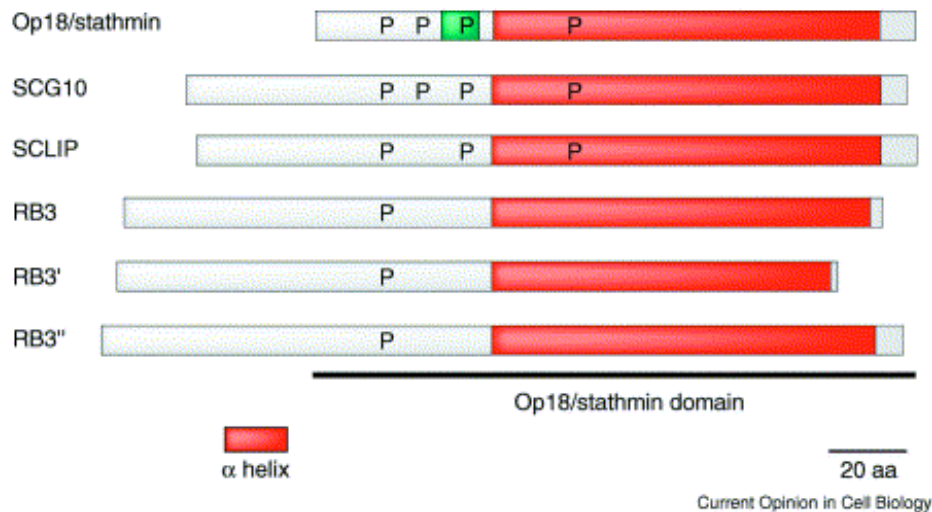


Figure 9. (adapted from Cassimeris, 2002) Schematic diagram of Op18/stathmin and related proteins. SCG10, SCLIP, RB3, RB3' and RB3'' are expressed in neurons and differ from Op18/stathmin by N-terminal extensions that are likely to target them to membranes (Ozon et al., 1997). The Op18/stathmin domain is highly conserved among all family members (~ 70% identical). The N-terminal region of Op18/stathmin contains a polyproline II helix (green box) while the remainder of the N-terminus is unstructured [Redeker et al.,2000; Wallon et al.,2000]. Most of the remaining protein is predicted to have a small alpha, Greek-helical structure (Gigant et al.,2000, Redeker et al, 2000; Wallon et al.,2000), shown here in red. When not bound to tubulin, this region also has a disordered structure (Steinmetz et al., 2000). The positions of serine phosphorylation sites in Op18/stathmin are shown. The conserved positions of serine residues present in the other family members are also shown.

Other members of the stathmin/op18 family are SCG10, SCLIP, RB3 and the two splice variants RB3' and RB3'' (Rowlands, Williams et al. 1995; Ozon, Maucuer et al. 1997; Charbaut, Curmi et al. 2001). These proteins are expressed in the nervous system and contain a domain which is highly homologous to stathmin/op18 but also additional N-terminal sequences probably anchoring them to membranes. All of them have microtubule destabilizing activity.

Stathmin/op18 and the other stathmin family members bind two tubulin-dimers per molecule (Belmont and Mitchison 1996) forming a complex termed T₂S. This interaction has significant impact on stathmin molecular structure. In solution it exists in a rapid equilibrium between a disordered structure and one containing a long α -helical structure (Steinmetz, Kammerer et al. 2000). Tubulin binding stimulates folding of a large region of stathmin/op18 into a long, extended α -helix, similar to that found in the RB3-tubulin crystal (Gigant, Curmi et al. 2000; Ravelli, Gigant et al. 2004).

Two different mechanisms for microtubule destabilization by stathmin/op18 have been proposed *in vitro*. It either acts by sequestering free tubulin on the expense of the pool of polymerized tubulin, or it directly induces catastrophes at microtubule plus ends. Catastrophe promotion seems to require GTP hydrolysis at microtubule tips (Howell, Larsson et al. 1999). It has been hypothesized from the crystal structure of the RB3-tubulin complex (Gigant, Curmi et al. 2000; Ravelli, Gigant et al. 2004) that stathmin interaction with microtubules at the tips could introduce a curvature into the protofilaments that make them peel away from the microtubule. In addition it could disrupt lateral and longitudinal contacts of the individual protofilaments destabilizing the microtubule tips.

It is unclear to which extent each of these mechanisms contributes to stathmin/op18 destabilizing activity *in vivo* (Cassimeris 2002).

Stathmin/op18 activity is modified by phosphorylation in response to various signals regulating cell proliferation and differentiation (Sobel 1991) as well as cell cycle progression (Larsson, Melander et al. 1995; Marklund, Larsson et al. 1996; Melander Gradin, Marklund et al. 1997; Gradin, Larsson et al. 1998). Mammalian stathmin/op18 gets phosphorylated at up to four sites including Ser16, Ser25, Ser38 and Ser63. The *Xenopus* pro-

tein lacks Ser63 and thus only contains three phosphorylation sites (Maucuer, Moreau et al. 1993; Andersen, Ashford et al. 1997). Phosphorylation turns off stathmin/op18 destabilizing activity possibly by decreasing stathmin-tubulin interaction and/or catastrophe promotion (Di Paolo, Antonsson et al. 1997; Holmfeldt, Larsson et al. 2001).

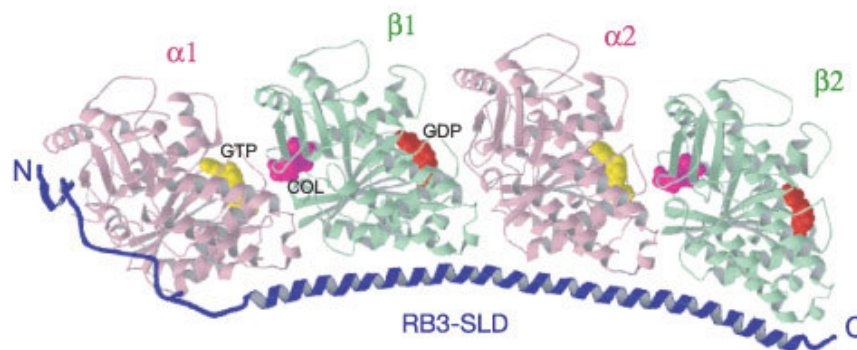


Figure 10. (adapted from Ravelli et al., 2004). The tubulin–colchicine: RB3-SLD complex. The complex includes two tubulin alphabeta heterodimers, with colchicine bound to beta subunits at the interface with alpha.

There is certain indication that the site-specific pattern of phosphorylation determines the degree of stathmin/op18 activity: Phosphorylation at Ser16 and Ser63 inhibits stathmin/op18 to a greater extent than at phosphorylation at Ser25 and Ser38 (Di Paolo, Antonsson et al. 1997; Horwitz, Shen et al. 1997; Larsson, Marklund et al. 1997; Gradin, Larsson et al. 1998).

II. Aim of the thesis

Polarized growth of microtubules is hypothesized to be one of the major principles contributing to selforganization of microtubules into functional arrays. Evidence for this principle is mainly based on data derived from functional microtubule growth assays as well as computer simulations. However, the biochemical mechanisms which regulate polarized growth are poorly understood.

It was proposed that gradients of diffusible regulative activities could create a cytoplasmic microenvironment of graduated microtubule stabilizing activity. Such a mechanism would provide a plausible explanation for the phenomenon of polarized growth. However, experimental evidence supporting this idea was missing so far.

Therefore, the major aim of this thesis was to test directly if graduated microtubule regulating activities exist in cells. Since stathmin/op18 had been previously implicated in local microtubule stabilization during cell migration and mitosis, we decided to monitor the local activity of this protein in cells. The microtubule destabilizing activity of stathmin correlates with its ability to interact with tubulin. Thus, we constructed a FRET based sensor that was able to non-invasively report changes in stathmin-tubulin interaction and introduced this sensor into cells.

III. Results

A. Detection of stathmin-tubulin interaction *in vitro*

Stathmin-tubulin interaction and stathmin's microtubule destabilizing activity was shown to be phosphorylation dependent (Di Paolo, Antonsson et al. 1997). Previous approaches utilizing phosphospecific stathmin antibodies to analyze stathmin phosphorylation in cells (Gavet, Ozon et al. 1998) suffered from an intrinsic drawback: The antibody fluorescence signal integrates both, local stathmin concentration and phosphorylation. Unfortunately, it is impossible to deduce local stathmin phosphorylation specifically from such a composite fluorescence signal.

Thus, we decided to design FRET sensors, which can assess stathmin phosphorylation as a function of stathmin-tubulin interaction. Initially, we tested two different FRET-based approaches *in vitro*. Afterwards, one of these sensors was used to monitor stathmin-tubulin interaction *in vivo*.

A1. Two component system: GFP-stathmin & Rhodamine-tubulin

A straightforward way to assess stathmin-tubulin interaction by means of FRET is to label the two interacting proteins with different fluorophores.

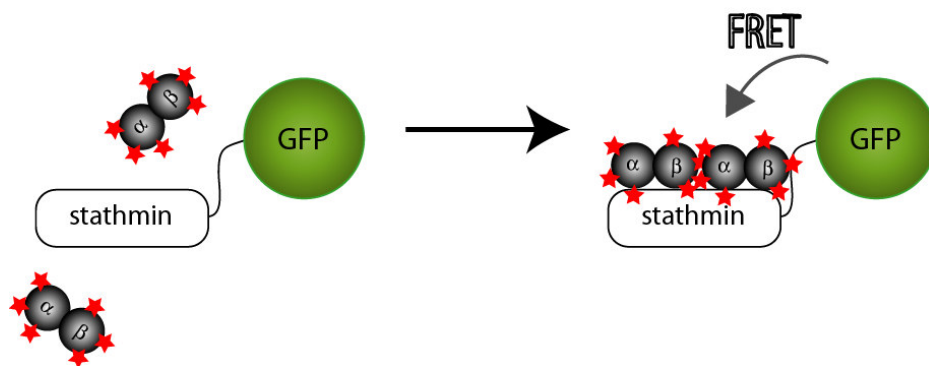


Figure 1. Schematic representation of the two-component FRET system to detect stathmin-tubulin interaction.

Interaction will then be indicated specifically by an increase of FRET since it brings the two fluorophores into close proximity (<8nm). For this purpose we decided to use a stathmin labeled with green fluorescence as FRET-donor and tubulin labeled with red fluorescence as FRET-acceptor (Figure 1).

A His-tagged version of *Xenopus* stathmin was genetically fused with its N-terminus to an enhanced green fluorescent protein (EGFP) and the fusion construct was expressed in *Escherichia coli* (Figure 3A). Purified pig-brain tubulin was chemically labeled with 5-(6)-carboxytetramethylrhodamine, succinimidyl ester (5(6)-TAMRA), a red fluorescent dye that covalently couples to free amino groups (Figure 2).

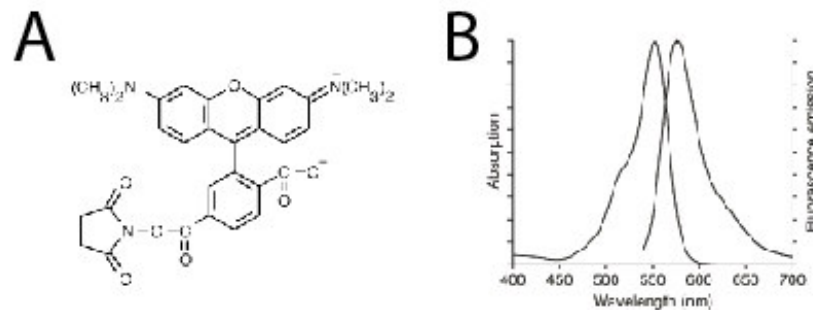


Figure 2. (A) 5(6)-carboxytetramethylrhodamine, succinimidyl ester (5(6)-TAMRA, SE) is a red fluorescent dye that covalently reacts with free amino groups. It can be used for fluorescent labeling of proteins. **(B)** TAMRA absorption/emission spectrum at pH 7.0.

In order to analyze, if FRET between GFP-stathmin and TAMRA-tubulin (R-tubulin) was taking place, we monitored the GFP-donor-emission in response to addition of increasing amounts of R-tubulin with a spectrofluorometer (Figure 3).

We could observe successive quenching of donor emission as a function of acceptor concentration indicating that FRET was indeed taking place between the two labeled components in solution. After the R-tubulin heterodimer concentration reached about double the GFP-stathmin concentration ($\approx 4 \mu\text{M}$), donor emission quenching was hardly detectable anymore indicating that most of the GFP-stathmin molecules were satu-

rated with R-tubulin. This finding is in line with the known 1:2 stoichiometry of stathmin-tubulin interaction (Belmont and Mitchison 1996).

Additionally we tested, if the GFP-stathmin-tubulin-interaction was impaired by phosphorylation as reported for the interaction between unmodified stathmin and tubulin (Horwitz, Shen et al. 1997).

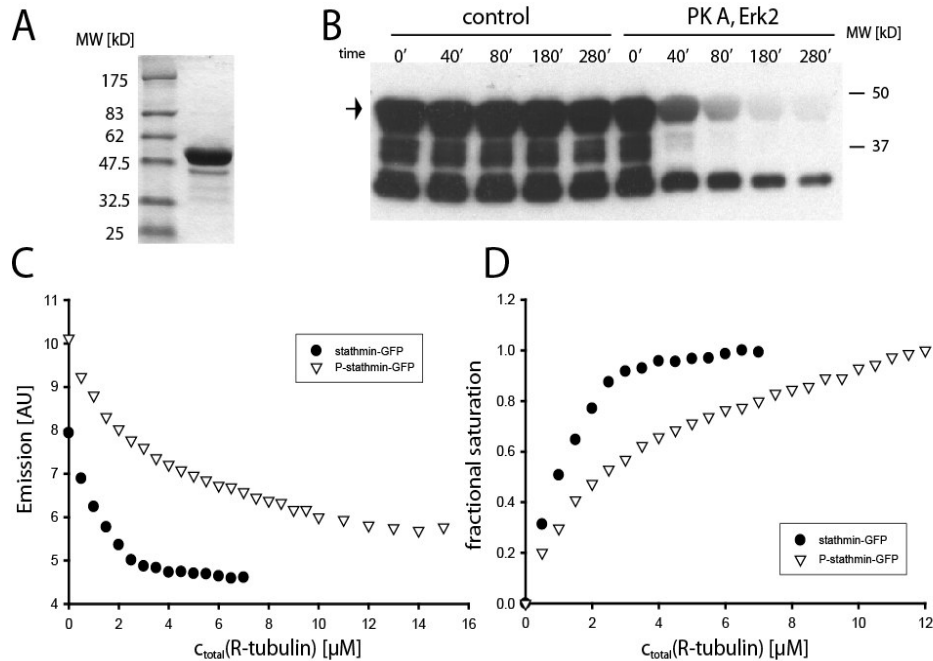


Figure 3. (A) Coomassie staining of purified, recombinant 6-His-tagged GFP-stathmin (right lane) and molecular weight marker (left lane). The calculated molecular weight of GFP-stathmin is 45188 D. (B) *In vitro* phosphorylation of GFP-stathmin by PK A and Erk2. Western blot was probed with anti-stathmin antibody that does not recognize the phosphorylated protein. Increase in phosphorylation is indicated by a decreasing amount of non-phosphorylated GFP-stathmin (arrow) in the presence of active kinases (PKA, Erk2). (C) Titration of R-tubulin into a 2 μM solution of unmodified (black circles) and phosphorylated (P-stathmin-GFP, white triangles) GFP-stathmin. After addition of ~ 4 μM R-tubulin, the FRET changes get minor indicating that all tubulin binding sites of unphosphorylated stathmin are occupied. (D) Stathmin-tubulin interaction represented as fractional saturation of stathmin versus total R-tubulin concentration.

Extracellular kinase 2 (Erk2) and protein kinase A (PK A) are known to phosphorylate stathmin (Beretta, Dobransky et al. 1993; Leighton, Curmi

et al. 1993; Di Paolo, Antonsson et al. 1997) on serine 16 (PK A consensus site), serine 25 (PK A consensus site, Erk2 consensus site), serine 38 (Erk2 consensus site) and Serine 63 (PK A consensus site, not present in the *Xenopus* protein). We performed an *in vitro* phosphorylation of stathmin using these two kinases (Figure 3B).

Phosphorylation of GFP-stathmin decreased its affinity to R-tubulin significantly (Figure 3D). However, it is difficult to directly derive a binding curve (fractional saturation versus free tubulin concentration) from these data, since binding of R-tubulin to stathmin gives a different FRET efficiency for each of the two binding sites, due to their different distance from the donor fluorophore. Nevertheless, these results show that the two-component system is basically capable to detect differences in stathmin-tubulin interaction as a function of stathmin phosphorylation. However, its application may be limited to reconstituted *in vitro* systems, because in cell or a *Xenopus* egg extract, endogenous, non-fluorescent tubulin is present already at high concentrations ($\approx 15 \mu\text{M}$). It would form "dark" complexes with GFP-stathmin thereby decreasing the dynamic range of the FRET signal.

Therefore, in order to increase the chance of donor/acceptor complex formation, it would be necessary to add high amounts of fluorescently modified tubulin into the system. However, this modified tubulin is known to disturb microtubule dynamics significantly when added in more than just tracing amounts. Thus, in view of a desired *in vivo* applicability, we developed an alternative approach to detect stathmin-tubulin interaction.

A2. One component system: COPY

Stathmin-tubulin association has an interesting feature: The free, unbound stathmin in solution has a rather flexible structure that becomes stiff and longitudinally extended upon binding of two tubulin heterodimers (Steinmetz, Kammerer et al. 2000). We took advantage of this feature by constructing a one-component FRET-sensor that detects stathmin-tubulin interaction via this conformational change: Cyan fluorescent protein (CFP) as a FRET-donor and Citrine (Griesbeck, Baird et al. 2001), a pH-stable variant of the yellow fluorescent protein (YFP) as a FRET-acceptor were fused genetically to the C- and N-terminus of *Xenopus* stathmin, respectively. When tubulin binds to COPY (CFP-OP18-YFP), the two fluorophores should move apart (>8 nm) resulting in a FRET decrease (Figure 4).

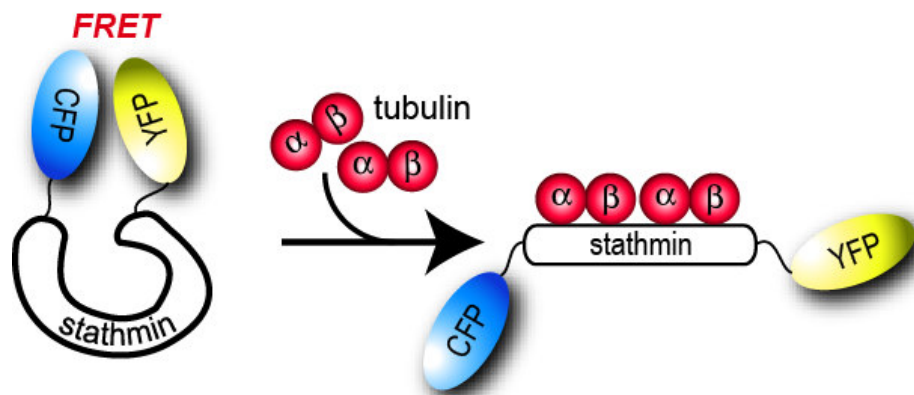


Figure 4. Schematic representation of COPY function: Binding of two tubulin heterodimers to COPY is indicated by a decrease of FRET.

Additionally, COPY mutants were generated, in which the three serines that are targets for stathmin phosphorylation were mutated either to alanine (COPY-aaa) to inhibit phosphorylation, or to glutamate (COPY-eee) to mimic it.

In order to test the functionality of these sensors, we expressed and purified them from *E.Coli* (Figure 5A) and examined whether the addition of tubulin to a solution of COPY resulted in the expected decrease of FRET indicated by an increase (“dequenching”) of donor fluorescence.

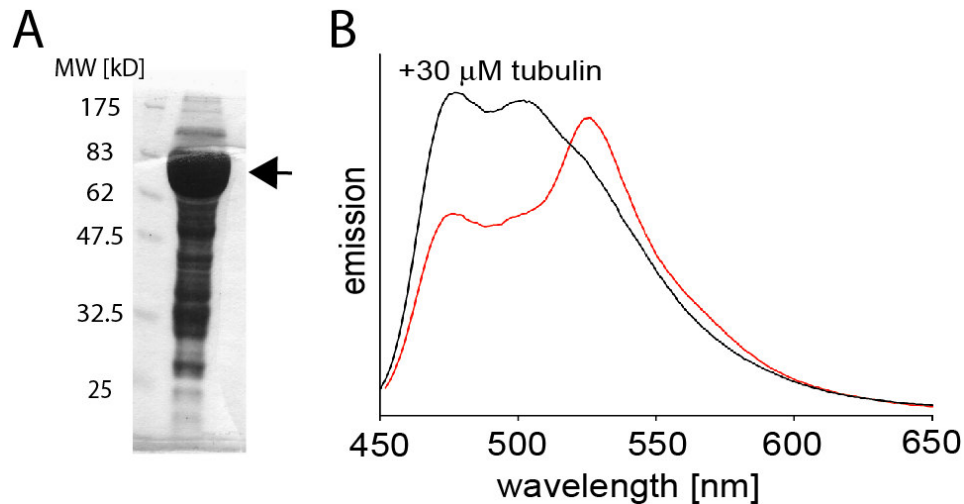


Figure 5. (A) Coomassie staining of recombinant His-tagged COPY (right lane, arrow). The calculated molecular weight for COPY is 72570 D. **(B)** Emission spectrum of 2 μM COPY-wt in BRB80 before (red curve) and after addition of 30 μM tubulin (black curve) recorded with a spectrofluorometer at room temperature.

The emission spectra of COPY confirmed the proposed behavior indicating high FRET of the sensor in the tubulin-free state and apparently no FRET in the tubulin-bound state (Figure 5B).

As a next step, we examined whether COPY would successfully mimic the behavior of unmodified stathmin concerning binding stoichiometry and phosphorylation dependence. Therefore, we titrated unlabeled tubulin into a solution of 4 μM COPY, excited the CFP emission at 450 nm and recorded the ratio of the YFP/CFP-emission-peaks (525 nm / 475 nm) using a spectrofluorometer. FRET correlates with a decrease of donor-fluorescence (“quenching”) and a concomitant increase in acceptor-fluorescence (“sensitized emission”). The YFP/CFP-ratio thus indicates changes in FRET with high sensitivity. Importantly, this ratio-signal is not dependent on sensor concentration since donor- and acceptor fluoro-

phores are present within the same molecule. Although dilution of the sensor decreases the absolute fluorescence intensities of both CFP and YFP, it does not affect the ratio of both.

As expected, the YFP/CFP-ratio decreased upon addition of up to 8 μM unlabeled tubulin almost linearly and then plateaued. This reflects saturation at the typical 1:2 binding stoichiometry of stathmin-tubulin interaction (Figure 6).

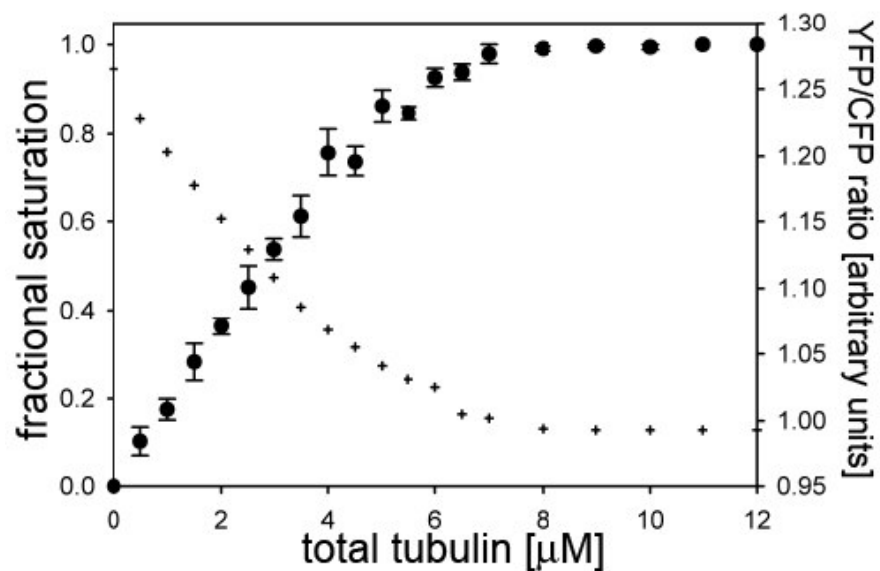


Figure 6. Increasing amounts of tubulin were titrated into a 4 μM solution of COPY-wt. A loss of FRET was detected by a decrease of the YFP/CFP-emission-ratio (crosshairs, right axis). After addition of $\sim 8 \mu\text{M}$ tubulin no further decrease could be detected. The changes in FRET are correlated with the fractional saturation (Y) defined as the ratio of occupied versus total binding sites of COPY (black circles, left axis). Full saturation of COPY was achieved at $\sim 8 \mu\text{M}$ tubulin as indicated by the minimum in YFP/CFP-emission ratios (fractional saturation=1), precisely reflecting the molar stathmin-tubulin interaction stoichiometry previously described (Jourdain, Curmi et al. 1997). Addition of buffer control, rabbit IgG, BSA or recombinant stathmin instead of tubulin did not affect the YFP/CFP-emission ratios (data not shown). Error bars show S.E.M. of four independent data sets.

In order to investigate how phosphorylation influences the COPY-tubulin interaction, we compared stathmin-tubulin interaction for all our COPY

mutants (COPY-aaa, COPY-eee) as well as for COPY-wt that had been *in vitro* phosphorylated by PK A and Erk2 (Figure 7A) as described previously for GFP-stathmin. From the ratio data we derived the corresponding binding curves (Figure 7B) and tested their fit to various binding models (single binding site, two independent binding sites, two cooperative binding sites). We found no evidence for cooperativity (Segerman, Larsson et al. 2000) in the COPY-wt-tubulin binding isotherms. By contrast, the data fitted well with a two independent site binding model with different affinities: one low ($K_{d1}=1.94 \pm 0.63 \mu\text{M}$) and one high affinity ($K_{d2}=0.020 \pm 0.015 \mu\text{M}$).

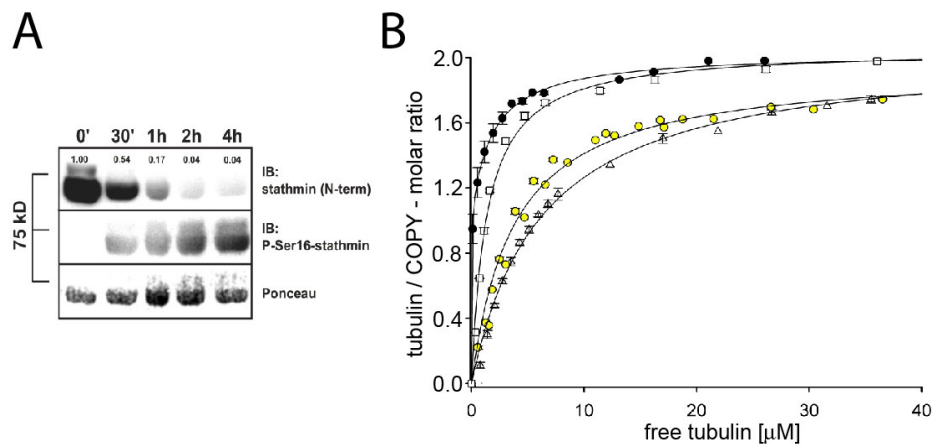


Figure 7. (A) Timecourse aliquots (0', 30', 1h, 2h, 4h) of the phosphorylation reaction were subjected to SDS-PAGE and western blot analysis using a stathmin antibody directed against an N-terminal epitope (upper panel) and phosphorylated Ser16 (middle panel). Ponceau staining of the western blot membrane confirms equal protein loading (lower panel). The N-terminal stathmin antibody was subsequently applied without prior stripping to the P-Ser16-stathmin antibody and only bound to COPY that had not been previously recognized by the phosphospecific antibody. The fraction of non-phosphorylated protein was quantified densitometrically (small numbers, upper panel). **(B)** Tubulin binding of 2 μM pseudo-phosphorylated COPY-eee, (white triangles), phosphosite-deficient COPY-aaa (white squares), COPY-wt (black circles) and phosphorylated COPY-wt (yellow circles) fitted with a two site binding model. Error bars represent the S.E.M. of at least two data sets.

Interestingly, *in vitro* phosphorylated COPY-wt as well as COPY-eee-tubulin binding exhibited a lower affinity for tubulin with two identical

binding sites ($K_{d\text{-wt}}=3.78 \pm 0.16 \mu\text{M}$, $K_{d\text{eee}}=6.25 \pm 0.27 \mu\text{M}$). Pseudo-phosphorylated COPY-eee thus mimicked the binding behavior of *in vitro* phosphorylated COPY (Beretta, Dobransky et al. 1993; Leighton, Curmi et al. 1993; Di Paolo, Antonsson et al. 1997). The COPY-aaa mutant also exhibited identical binding sites with slightly decreased average affinity ($K_{d\text{aaa}}=1.36 \pm 0.06 \mu\text{M}$) towards tubulin relative to the COPY-wt. No change in the YFP/CFP-emission-ratio was detected during phosphorylation of COPY-wt in the absence of tubulin (data not shown).

The mean K_d of COPY-wt-tubulin interaction corresponds well to the dissociation constant previously determined for the interaction of unmodified stathmin (or “non fluorescent”) with tubulin by plasmon resonance ($K_d=0.56 \pm 0.05 \mu\text{M}$, (Curmi, Andersen et al. 1997)). This indicates that COPY conveniently mimics the binding characteristics of unmodified stathmin.

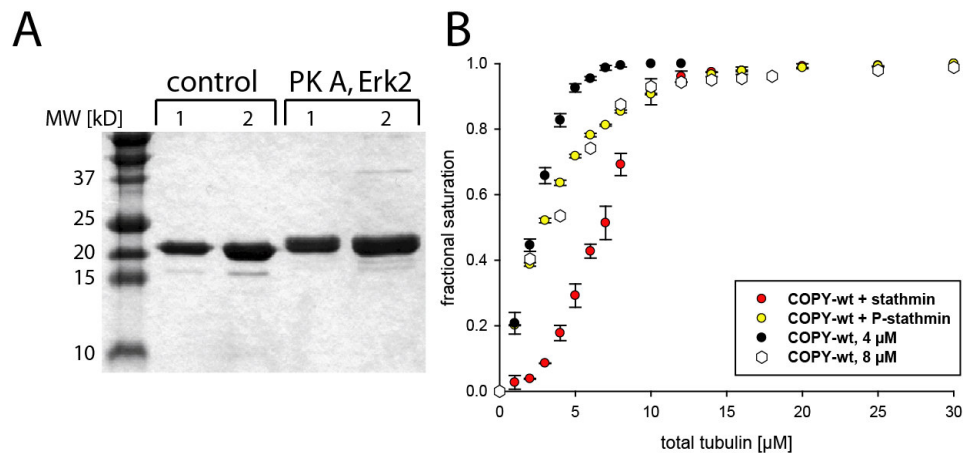


Figure 8. (A) Coomassie staining of non-phosphorylated (control) and *in vitro* phosphorylated, recombinant His-tagged stathmin (PK A, Erk2) and molecular weight marker (left lane). Hyperphosphorylation decreased stathmin mobility in an SDS-PAGE-gel as indicated by a band-shift of phosphorylated stathmin relative to the control. The numbers above the lanes indicate different amounts of each sample that was loaded onto the gel for analysis. **(B)** Competition of 4 μM COPY-wt with non-phosphorylated (red circles) and 4 μM phosphorylated (yellow circles) stathmin for tubulin binding represented as a plot of fractional saturation versus total tubulin concentration. Plot of COPY-wt-tubulin interaction (4 μM COPY: black circles; 8 μM COPY: white hexagons) was added to the graph for comparison. Error bars represent the S.E.M. of two data sets.

In order to evaluate how GFP fusion affected stathmin's tubulin binding abilities, we carried out a competition experiment: The YFP/CFP-emission-peak-ratio of a mixture of 4 μM COPY-wt with 4 μM stathmin or 4 μM P-stathmin, respectively, was recorded in response to the addition of increasing amounts of unlabeled tubulin. As expected the curve for the 4 μM stathmin / 4 μM COPY mixture reached saturation at $\sim 16 \mu\text{M}$ added tubulin (Figure 8B). At lower tubulin concentrations, the curve showed delayed fractional saturation of COPY as indicated by the convex shape. This suggests that the affinity of unmodified stathmin to tubulin is higher to a certain degree than that of COPY to tubulin. Thus, at low tubulin concentrations unmodified stathmin efficiently "catches" away the heterodimers from COPY. The convex shape was not observed when unmodified stathmin had been previously phosphorylated *in vitro* (yellow circles) confirming that phosphorylation considerably decreases its tubulin binding affinity as previously reported (Di Paolo, Antonsson et al. 1997).

In conclusion, COPY seems to have a lower affinity for tubulin compared to unmodified stathmin most probably due to its GFP fusions. Nevertheless, the sensor precisely mimics two of the key features of stathmin-tubulin interaction, which are the 1:2 binding stoichiometry as well as phosphorylation dependence. Thus it is a suitable probe for detecting stathmin phosphorylation in an *in vivo* system.

A3. Summary

We tested two different kinds of FRET-based sensors for their ability to detect stathmin-tubulin interaction: GFP-stathmin and R-tubulin as a FRET-pair, and COPY as a single component conformational FRET-sensor. Both systems turned out to specifically detect stathmin-tubulin interaction *in vitro* as indicated by the typical 1:2 binding stoichiometry and phosphorylation dependence.

Since the two-component system requires the addition of unphysiological high amounts of labeled tubulin to a system to yield a reasonable dynamic range for a FRET signal, we continued our *in vivo* studies with COPY.

B. COPY detects phosphorylation dependent stathmin-tubulin interaction in *Xenopus* Egg extracts

In order to test phosphorylation dependent tubulin release of the sensor under more physiological conditions, we compared ratio images of a mitotic *Xenopus* egg extract (Murray 1991) supplemented with 6 μ M COPY-wt after incubation with okadaic acid (OA) and a untreated control extract (Figure 9). Okadaic acid is a strong inhibitor of protein phosphatase 2A (PP2A) and known to induce hyperphosphorylation of stathmin and to strongly promote microtubule polymerization in mitotic *Xenopus* egg extracts (Andersen, Ashford et al. 1997). We found a $10.5 \pm 0.87\%$ (\pm S.E.M, n=2) higher YFP/CFP-ratio for the okadaic acid-treated sample compared to the untreated control extract. This indicates that inhibition of phosphatases induces a tubulin-release from COPY that can be detected by our probe, reflecting the previously reported hyper-phosphorylated state of stathmin in okadaic acid-treated extracts.

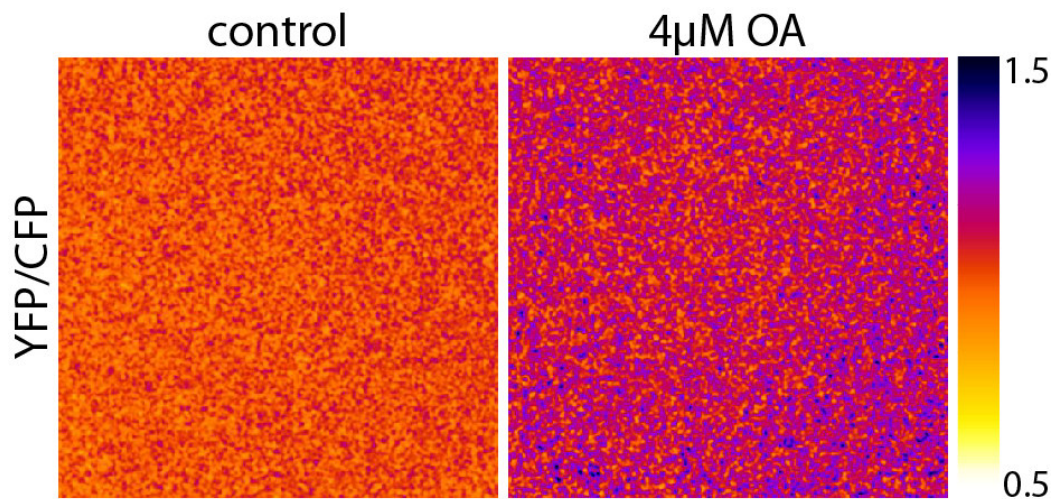


Figure 9. Ratio-images of COPY-wt (6 μ M) added to mitotic *Xenopus* egg extract subjected to okadaic acid treatment (4 μ M OA, right panel) versus untreated extract (control, left panel). Color bar corresponds to the ratio values in the images.

C. Illuminating stathmin-tubulin interaction in cells

Having confirmed the functionality of COPY *in vitro* and in *Xenopus* egg extracts, we now used this tool to monitor stathmin-tubulin interaction in *Xenopus* cells.

C1. Characterizing exogenous stathmin expression in cells

C1.1. Expression level

We introduced our fluorescently modified stathmin fusions into *Xenopus* A6 fibroblasts by transfection.

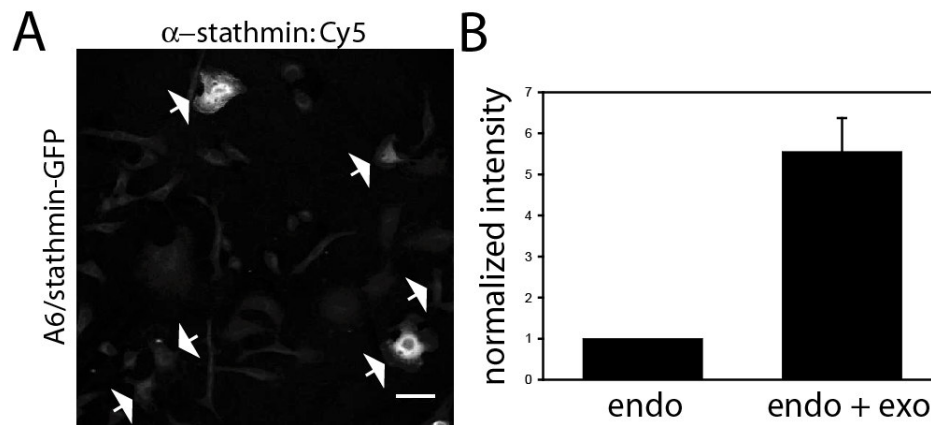


Figure 10. (A) Immunostaining of endogenous and exogenous stathmin using a primary anti-stathmin and a secondary Cy5-labeled antibody (α -stathmin: Cy5). Expressing cells (arrows) were identified by their GFP emission (not shown). Scale bar corresponds to 40 μ m. (B) Exogenous GFP-stathmin expression in cells (endo+exo) normalized to endogenous stathmin expression (endo). Error bar corresponds to S.E.M of the expression differences within nine different images.

In order to estimate the relationship of endogenous versus exogenous stathmin protein yielded with this procedure, we quantified the expression by comparing stathmin levels in transfected and non-transfected cells using anti-stathmin immunostaining (Figure 10A).

It turned out that the exogenous protein was expressed about five times over the endogenous stathmin level (Figure 10B). The cells seemed to tolerate the overexpression well as indicated by their apparently unaltered morphology.

C1.2. Localization and Diffusion

Transfected COPY exhibited a cytoplasmic distribution. A localization of the protein on particular structures could not be observed. In order to confirm this, we determined the diffusion behavior of COPY in living cells by fluorescence recovery after photobleaching (FRAP). We bleached small circular regions of YFP-fluorescence in transfected cells and monitored the kinetics of diffusion of unbleached material into this region (Figure 11).

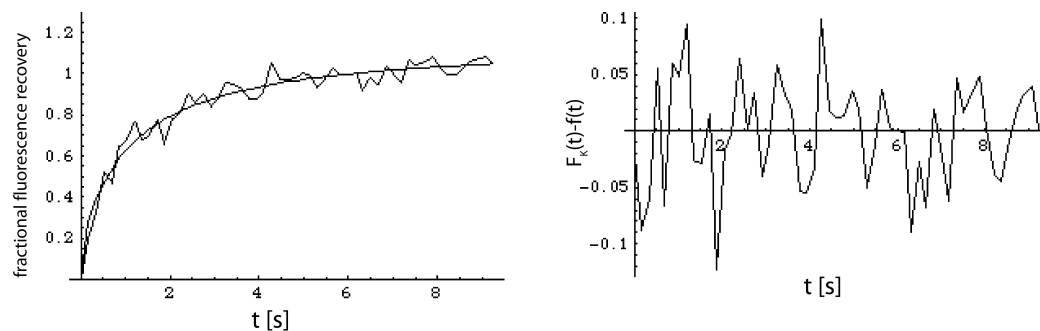


Figure 11. YFP-Fluorescence recovery after photobleaching in COPY-wt transfected *Xenopus* A6 fibroblasts. Plot shows a fractional fluorescence recovery curve ($F_K(t) = (F_K(t) - F_K(0)) / (F_K(\infty) - F_K(0))$) fitted with $f(t) = \exp(-2\tau_D/t) [I_0(2\tau_D/t) + I_1(2\tau_D/t)]$ to obtain τ_D with I_0 and I_1 being modified Bessel functions. The diffusion constant D derives from $\tau_D = \omega^2/4D$ with ω being the radius of the bleaching beam. The recovery curve (left panel) shown here is an average curve from two different bleaching experiments. Fit residuals are shown in the right panel.

Bleaching instantly induced a decrease in total fluorescence intensity of the whole cell, indicating that exchange of fluorescent material by diffusion was happening faster than the temporal resolution of data recording in our experimental setup. As a consequence, the experimental data curve was deficient of the steep, initial part of fluorescence recovery and fitting thus underestimated the actual diffusion constant. Nevertheless, this calculation indicated with $D \approx 2 \mu\text{m}^2/\text{s}$ the lower range of plausible values. The actual diffusion constant is thus likely to lie between $2 \mu\text{m}^2/\text{s}$ and $15 \mu\text{m}^2/\text{s}$, latter being the diffusion constant of the GFP.

In addition, we analyzed the co-distribution of CFP-stathmin with YFP (Citricine) as a cytoplasmic marker in co-transfected *Xenopus* A6 cells (Figure 12). The YFP/CFP-emission-ratio images indicated that CFP-stathmin co-distributed very well with YFP throughout the cytoplasm but not in the nucleus that was not permeable for CFP-stathmin probably because of size exclusion.

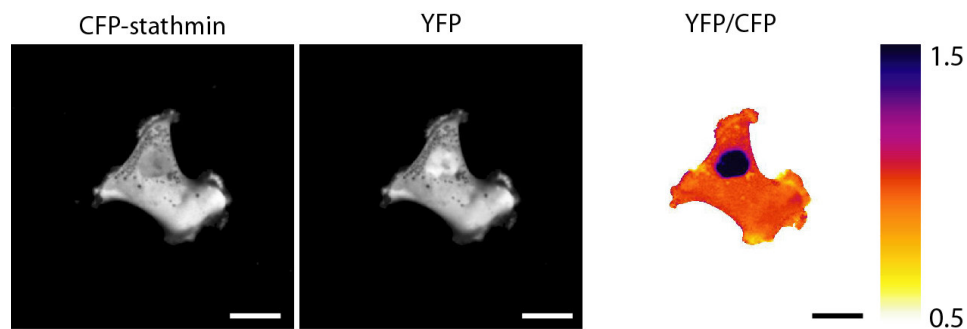


Figure 12. Co-distribution of CFP-stathmin and YFP (Citricine) co-transfected to *Xenopus* A6 fibroblasts. CFP-stathmin, but not YFP is excluded from the nucleus explaining the high YFP/CFP-ratio observed there. Scale bar corresponds to $20 \mu\text{m}$.

We quantified the level of co-distribution by applying a method of data evaluation that produced a single average parameter reflecting the degree of spatial inhomogeneity (SIH) of CFP-stathmin/YFP-co-distribution in a cell (Figure 13). Mean ratios within squares placed arbitrarily at the center and the four edges of each cell were measured.

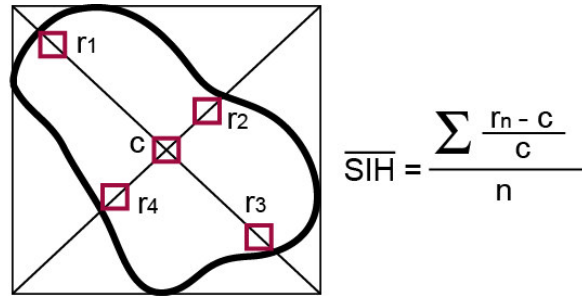


Figure 13. Schematic representation of the spatial inhomogeneity assay (SIH). A square was drawn to fit the ratio image of the cell. 10x10 pixel squares were placed at the sites, where the diagonals hit the edges of the cell (r1-r4) or each other (c) in the center. The mean ratio values in these squares were acquired. Relative ratiochanges $((r_n - c)/c)$ from the periphery to the inside were calculated and averaged for each cell. From these single cell SIH-values the average for the whole population was calculated.

We calculated the relative differences between the ratio in the central square and those in the four edges. From the mean SIH of each cell, an average SIH for the whole population of cells was derived. The SIH of eight different co-transfected was found to be close to zero ($SIH = 0.007 \pm 0.015$ (\pm S.E.M.)) indicating a homogenous distribution of CFP-stathmin relative to YFP along the center-periphery axis.

In conclusion, both the FRAP and the co-distribution experiments demonstrated that COPY freely diffuses within the cell.

C2. Stathmin-tubulin interaction gradients in interphase cells

In order to reveal local differences in stathmin-tubulin interaction within cells, we introduced COPY into *Xenopus* fibroblasts by transfection. Overexpression of COPY did not affect the microtubule cytoskeleton seriously although the tubulin network seemed slightly less dense (Figure 14). The YFP- and the CFP fluorescence images for each cell were acquired and their ratios calculated. High YFP/CFP-ratios (high FRET, blue color) correspond to the unbound state of COPY, whereas low YFP/CFP-ratios (low FRET, yellow color) represent the extended conformation of COPY when it is in a complex with tubulin heterodimers. Interestingly, COPY revealed spatial differences of stathmin-tubulin interaction within *Xenopus* A6 cells. Low interaction was most frequently detected within lamella that are typical for migrating cells. From these areas, the interaction increased towards the cell center.

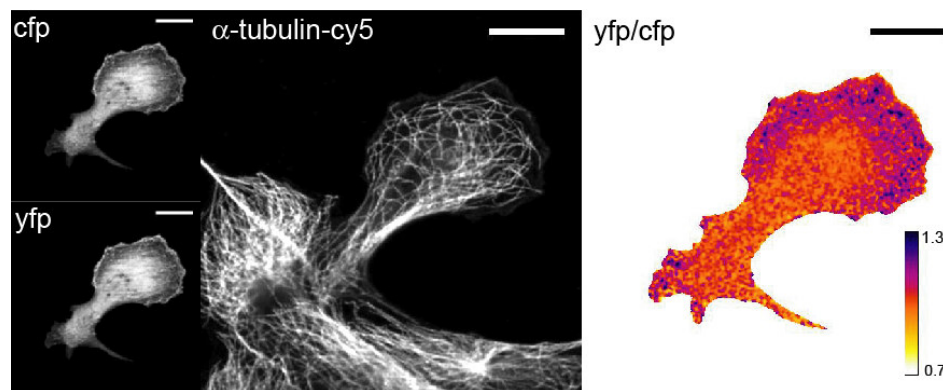


Figure 14. Fixed *Xenopus* A6 cell expressing COPY-wt. CFP- and YFP-emission images (left panel) were acquired simultaneously by confocal microscopy. The YFP/CFP-ratio images (right panel) were calculated by dividing the two channels. The color bar corresponds to the ratio values in the image. Microtubules (middle panel) were visualized using a monoclonal primary anti- α -tubulin antibody and a secondary Cy5-labeled anti-mouse antibody. The image shows a transfected cell neighbored by several untransfected ones. Scale bars correspond to 20 μ m.

As evident from our *in vitro* experiments (Figure 3, 7), a decrease of COPY-tubulin interaction could be attributed either to COPY phosphorylation or to a locally reduced tubulin concentration. In order to distinguish between the two phenomena, we compared the spatial patterns of stathmin-tubulin interaction in cells transfected with COPY-wt with those of cells expressing the phosphorylation site deficient mutant COPY-aaa using the SIH-assay (Figure 15).

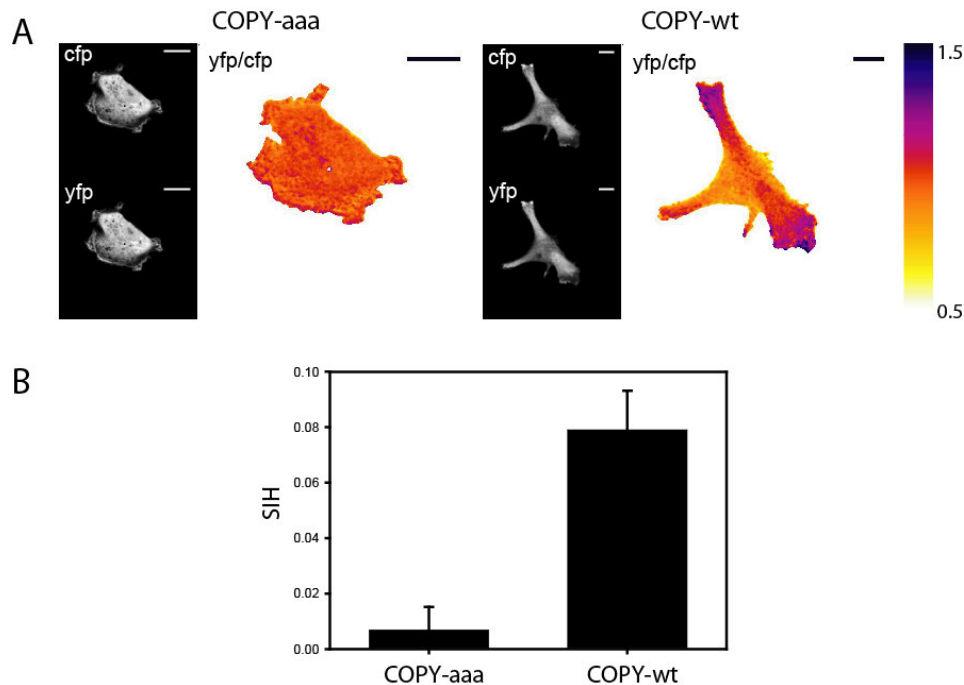


Figure 15. (A) CFP- and YFP-emission and YFP/CFP-ratio images of COPY-aaa (left panel) and COPY-wt (right panel) transfected live *Xenopus* A6 cells. Scale bars correspond to 20 μm . **(B)** Statistical evaluation of the spatial inhomogeneity of COPY-tubulin interaction in COPY-wt and COPY-aaa transfected populations of live *Xenopus* A6 cells (SIH-assay). Error bars correspond to the S.E.M. of at least 20 cells.

The SIH we observed for the COPY-wt live cell population was much higher than that measured for the COPY-aaa population indicating that phosphorylation contributed to the SIH observed in COPY-wt transfected cells. However, we could also observe spatial inhomogeneities in individual COPY-aaa expressing cells. Obviously, these latter patterns were not phosphorylation dependent and possibly a result of local differences in

the cellular tubulin concentration caused by local e.g. polymerization/depolymerization events.

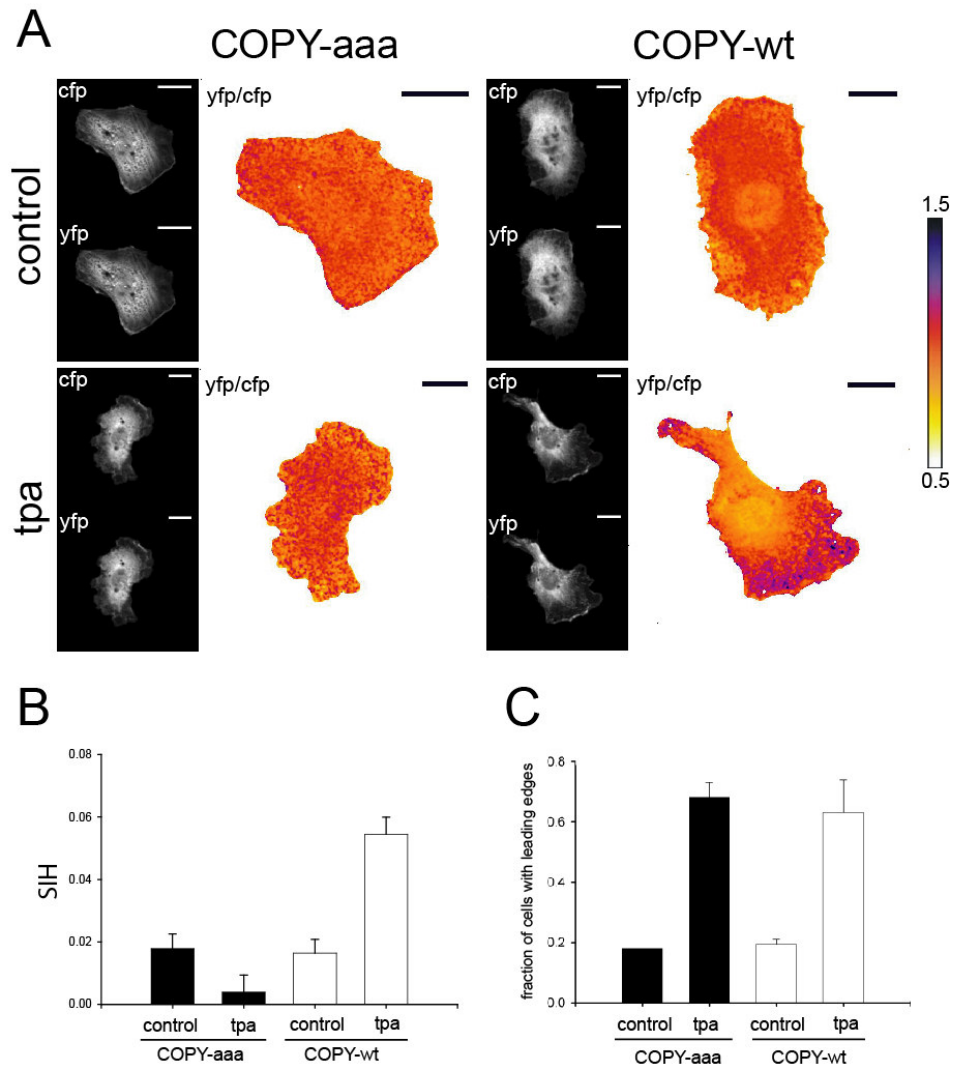


Figure 16. TPA induces phosphorylation dependent gradients of COPY-tubulin interaction. **(A)** *Xenopus A6* cells transfected with COPY-aaa (left column) and COPY-wt (right column). Cells were cultured for ~16 h in serum-free culture medium (upper row) or stimulated 30 min with 100 nM TPA (lower row). Images show the CFP- and the YFP-emission of COPY and their ratio. Scale bars correspond to 20 μ m. **(B)** SIH-assay of COPY-aaa (black bars) or COPY-wt (white bars) expressing *Xenopus A6* cells. Error bars show S.E.M. of at least 41 cells scored per population. Cells were sampled in three different transfection experiments **(C)** Induction of leading edges by TPA stimulation. Bars represent the fraction of COPY-wt (white bars) or COPY-aaa (black bars) transfected cells that show significant membrane ruffling at the leading edges. Error bars show S.E.M. of two different transfection experiments.

In addition, other unknown factors may regulate stathmin-tubulin interaction independent of phosphorylation.

The local differences in stathmin-tubulin interaction observed in *Xenopus* A6 cells grown under normal serum conditions appeared to be related to the formation of leading edges in motile cells. 12-O-tetradecanoylphorbol-13-acetate (TPA), a potent activator of protein kinase C, induces stathmin phosphorylation (Chneiweiss, Cordier et al. 1992; Drouva, Poulin et al. 1998) and stimulates membrane ruffling and cell motility. TPA induced membrane ruffling (Imamura, Takaishi et al. 1998; Okamoto, Kawano et al. 1999) is mediated by a Rac1 dependent pathway as is growth factor triggered stathmin phosphorylation (Daub, Gevaert et al. 2001). We treated serum starved *Xenopus* A6 cells expressing COPY-wt or COPY-aaa with TPA, fixed the cells and analyzed the SIH of COPY-tubulin interaction (Figure 16) as described above (Figure 13).

The serum starved unstimulated control cells revealed about the same low basal SIH-level, when transfected either with COPY-wt or COPY-aaa. In the presence of TPA we observed a roughly 3-fold SIH-increase within the population of COPY-wt cells (Figure 16B). Interestingly, TPA-stimulation induced a SIH-decrease within the COPY-aaa population. Phosphorylation of endogenous stathmin coupled to a local tubulin release is a plausible explanation for this result. Importantly, the COPY-tubulin interaction patterns observed in the presence of TPA appeared similar to those observed in COPY-wt cells grown in the presence of serum. Creation of COPY-tubulin interaction gradients by TPA was accompanied by the massive induction of leading edges and membrane ruffles (Figure 16C).

Alternatively, we performed acceptor photobleaching (Bastiaens, Majoul et al. 1996) of TPA treated cells, transfected with COPY-wt and its mutants (Figure 17). The maximal differences of FRET-efficiency between central and lamella-like regions were found in COPY-wt transfected cells whereas the spatial FRET distribution in the phosphorylation site mutants was more homogenous, as previously shown by means of ratio-imaging and SIH-assay (Figure 16). COPY-eee revealed the most homogenous distribution of tubulin interaction, in agreement with the fact that this mutant

neither can be phosphorylated nor interacts with tubulin very efficiently. Therefore, COPY-eee-tubulin interaction is less sensitive to differences in local tubulin concentration than COPY-aaa-tubulin interaction. Inhibition of protein phosphatase 1 and protein phosphatase 2 by high concentrations of okadaic acid flattened the intracellular differences in COPY-wt-tubulin interaction significantly compared to untreated COPY-wt transfected cells ($p=0.004$, t-test). Importantly, this observation together with that made for inhibition of phosphatases in *Xenopus* extracts (Figure 9) suggest that phosphorylation and in particular the balance of kinase and phosphatase activity modulates the spatial distribution of stathmin-tubulin interaction within cells.

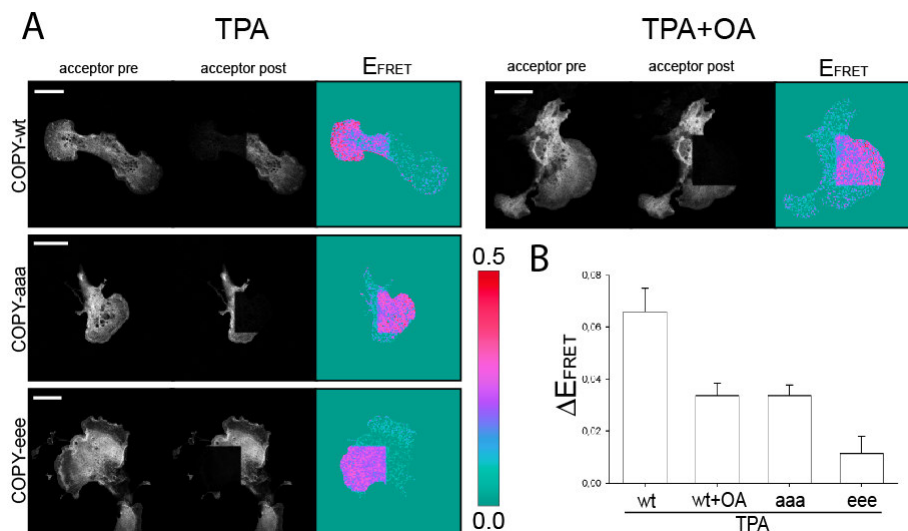


Figure 17. (A) Acceptor photobleaching of a COPY-wt (upper panel, left), COPY-aaa (middle panel, left), COPY-eee (lower panel, left) transfected, TPA (100 nM, 30 min) stimulated A6-cells. COPY-wt transfected cells were additionally treated with okadaic acid (6 μ M, 30 min, upper panel, right). Scalebars correspond to 20 μ m. **(B)** Mean differences in FRET-efficiency between the central and peripheral regions of the cells were quantified for each population of cells. Error bars correspond to the S.E.M of at least 18 cells per population.

The dynamic behavior of the gradients in TPA treated live cells was followed by timelapse ratio-imaging. Phosphorylation of stathmin fluctuated with time but was found preferentially in the lamellum. Retraction of

the lamellum at the end of the recording coincided with the disappearance of the gradient (Figure 18).

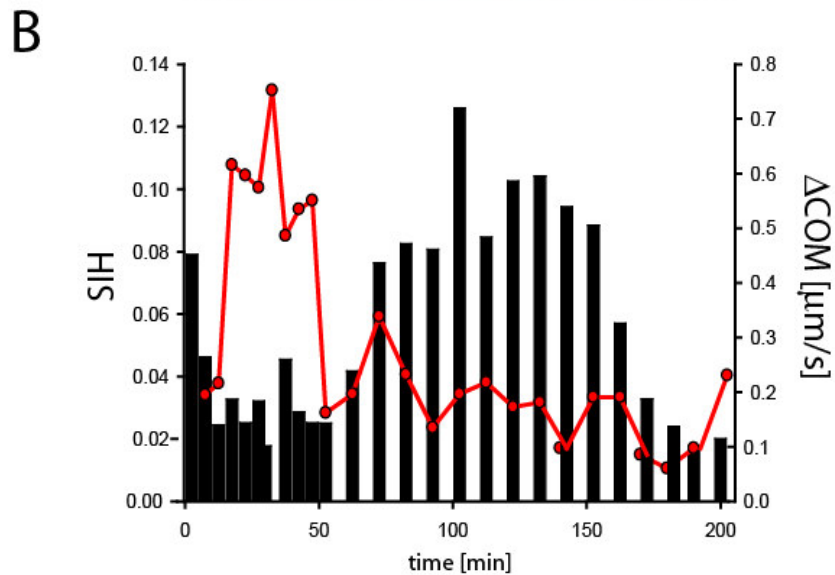
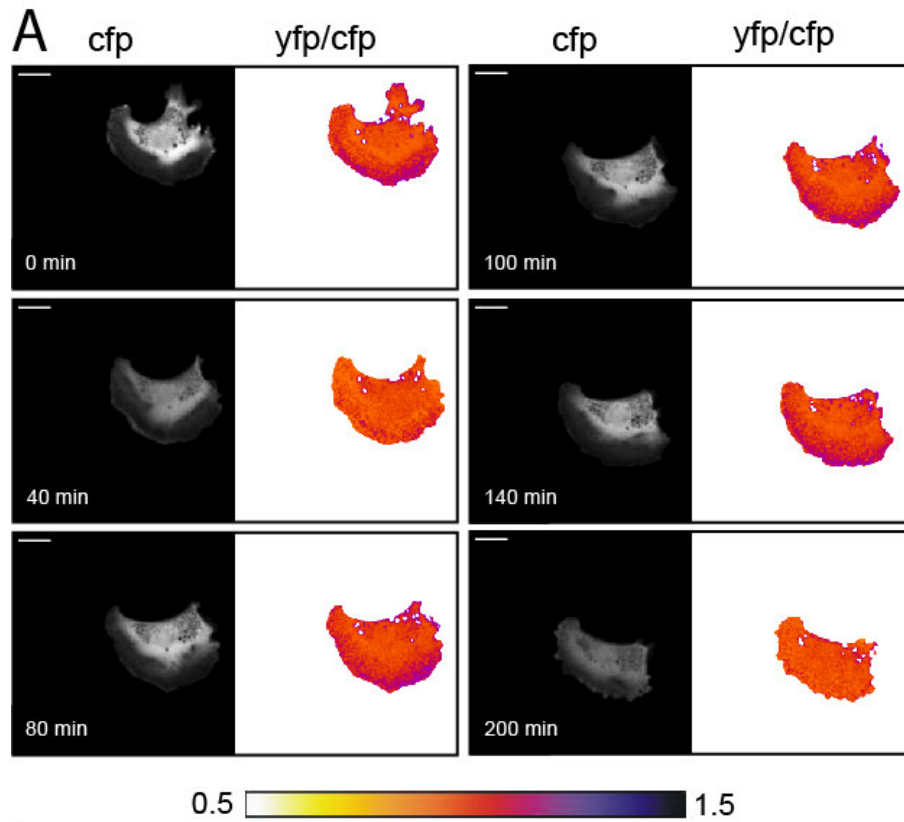


Figure 18. (A) Timelapse recording of YFP/CFP ratio in a COPY-wt transfected, TPA-stimulated A6 cell. Scalebars correspond to 20 μm . **(B)** SIH of ratio-timelapse (black bars, left axis) and center of mass displacement velocity (ΔCOM , right axis, red curve) versus timelapse progression.

Interestingly, stathmin phosphorylation seemed to precede cell movement as indicated by an anticorrelation of SIH and center-of-mass displacement velocity (Figure 18B).

C3. Stathmin-tubulin interaction gradients in mitotic cells

Stathmin was reported to be hyper-phosphorylated in mitotic *Xenopus* egg extracts in the presence of chromatin (Andersen, Ashford et al. 1997). This suggests the occurrence of a gradient of phosphorylation-inactivated stathmin around mitotic chromosomes. We tested this hypothesis by imaging COPY in mitotic cells. *Xenopus* XL177 cells were transfected with COPY-wt or COPY-aaa and the microtubules were visualized by immunostaining. Since Hoechst staining of DNA interfered with FRET detection by fluorescence bleed-through, chromosome position was inferred by the lower stathmin fluorescence intensity relative to the surrounding area.

We selected COPY-wt and COPY-aaa transfected cells in metaphase with similar expression levels as judged by fluorescence intensity. A COPY-tubulin interaction gradient was detected around mitotic chromosomes where tubulin sequestration increased with rising distance from the chromosomes (Figure 19). The interaction patterns observed within COPY-aaa transfected cells were flat indicating that the COPY-wt-tubulin interaction gradient was produced by stathmin phosphorylation around mitotic chromosomes.

Quantification of spindle morphology (Figure 20) suggests that phosphorylation of COPY-wt is crucial for the formation of proper spindles. The length of a spindle in an untransfected XL177 cell was $12.5 \pm 0.51 \mu\text{m}$ (\pm S.E.M.). Overexpression of COPY-wt decreased the length to $9.88 \pm 0.40 \mu\text{m}$ (\pm S.E.M.). This reduction was probably caused by incomplete inactivation of overexpressed COPY-wt. Apart from that, the spindles in COPY-wt cells looked normal. By contrast, the spindles of COPY-aaa transfected cells appeared seriously affected (Figure 20).

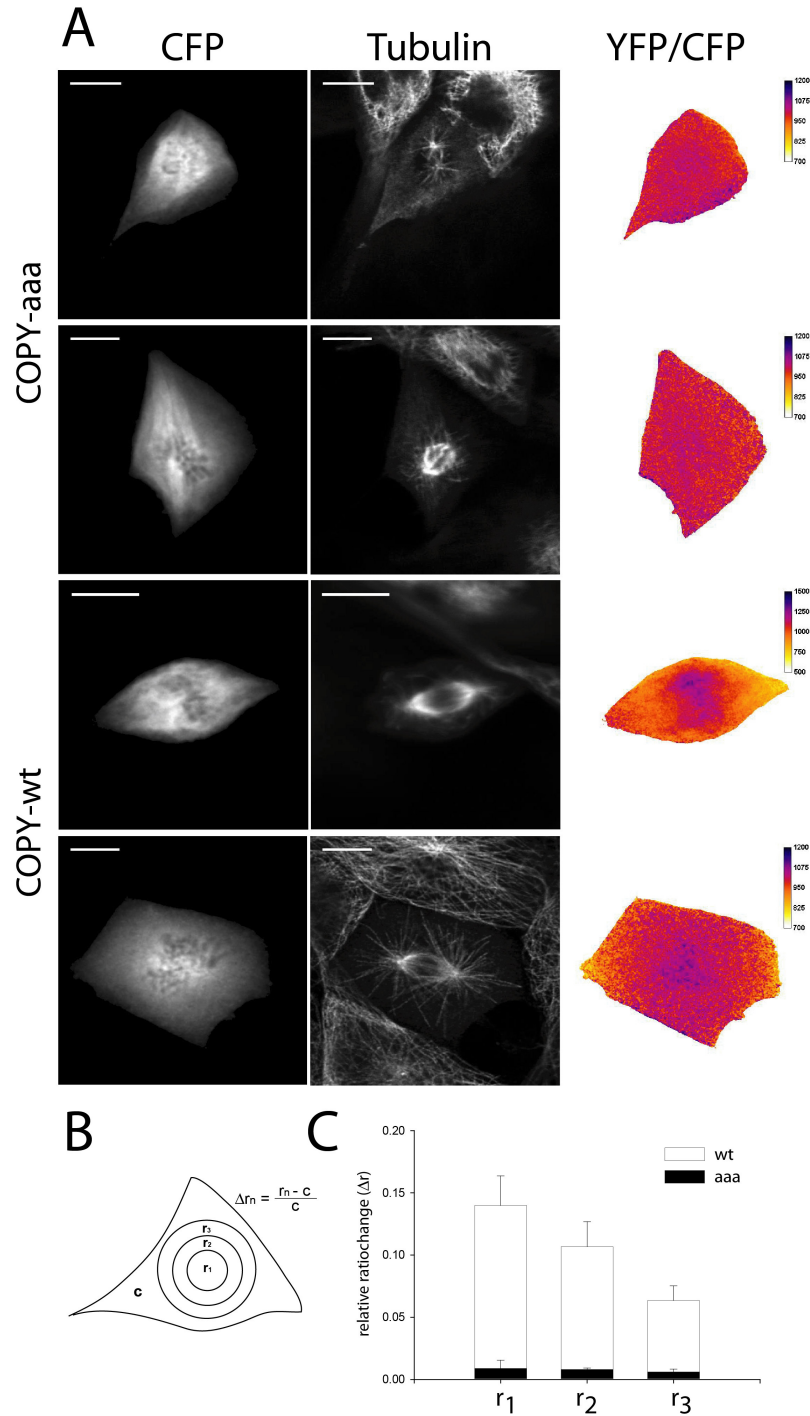


Figure 19. (A) *Xenopus* XL177 cells transfected with COPY-aaa or COPY-wt in mitosis. Note broader scale range of the first COPY-wt ratio-image (third panel from top). Scale bars correspond to 10 μ m. **(B)** Schematic representation of gradient analysis. Mean ratios were measured within three circular areas around the center of the spindle (r_1 - r_3). The mean ratio in the rest of the cell (c) was set as base value. The relative difference (Δr) between the basal ratio value and the mean ratio of the three circular regions was calculated. **(C)** Error bars show the S.E.M. of at least four cells scored per population.

Their size ($7.21 \pm 0.67 \mu\text{m}$ (\pm S.E.M.)) was decreased by $\sim 30\%$ compared to COPY-wt spindles and their morphology often looked perturbed.

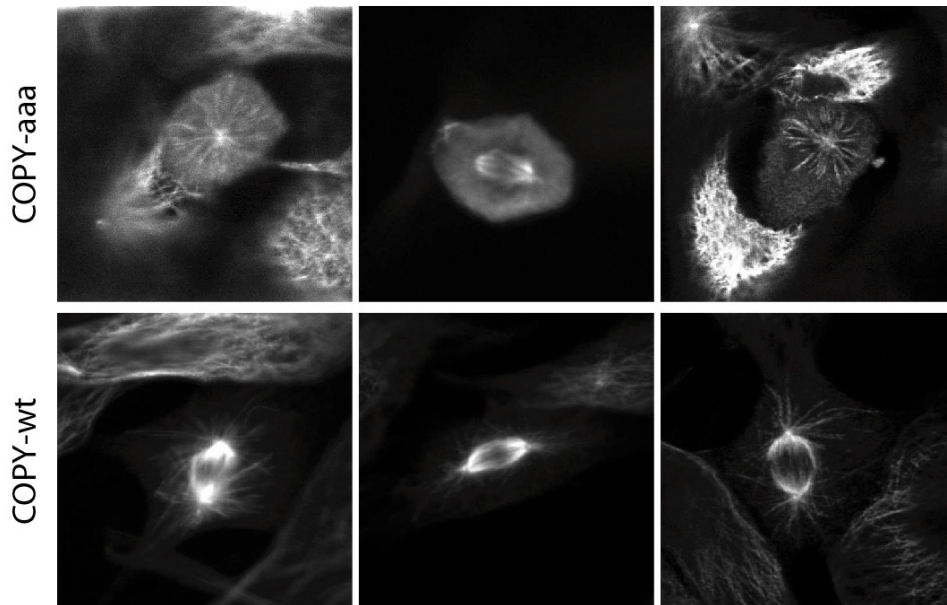


Figure 20. Tubulin immunostaining in COPY-aaa (upper panel) and COPY-wt (lower panel) transfected, mitotic XL177 cells. The phosphorylation mutant seriously perturbed spindle morphology.

In view of our results, this phenotype can be explained by a lack of stathmin inactivation around chromosomes. COPY-aaa exerted full depolymerizing activity resulting in shorter microtubules and in turn, smaller spindles. This observation is in line with previous studies which described a similar effect of the stathmin phosphorylation site mutant on mitotic spindles (Marklund, Larsson et al. 1996; Curmi, Andersen et al. 1997; Budde, Kumagai et al. 2001; Kuntziger, Gavet et al. 2001). We conclude that stathmin is phosphorylated and inactivated around mitotic chromatin in dividing cells and that this local inactivation is necessary for correct spindle assembly.

IV. Discussion

A. Stathmin-tubulin interaction gradients in interphase

Migrating cells exhibit a polarized microtubule cytoskeleton and polarized microtubule polymerization dynamics (Wittmann and Waterman-Storer 2001). A variety of regulatory proteins was implicated in the establishment of this polarity, among them APC, CLIP170 and the CLASP class of proteins. In this respect, a crucial upstream regulatory role was also assigned to the polarized activities of the Rho-GTPases Rac1 and RhoA.

A gradient of activated Rac1 at the leading edge of motile cells was visualized (Kraynov, Chamberlain et al. 2000) by FRET-based techniques. Pak1 kinase is a downstream effector of Rac1. Interestingly, upon growth factor stimulation (Sells, Pfaff et al. 2000) it gets specifically activated in the lamella of moving fibroblasts. Stathmin phosphorylation is known to be triggered via the Rac1-Pak1 pathway (Daub, Gevaert et al. 2001). Nevertheless, the fraction of phosphorylated stathmin is quite small (Daub, Gevaert et al. 2001) as revealed by bulk biochemical methods. Assuming a homogenous distribution of this fraction throughout the whole cell, its effect on global microtubule regulation is not expected to be dramatic. However, when specifically localized to a cellular compartment of small volume, its local concentration there could be high enough to exert significant effects on microtubule dynamics. Indeed, our FRET based stathmin-tubulin interaction sensor indicates locally enforced phosphorylation of stathmin in the lamella-like regions of motile interphase cells. These are extremely thin cellular protrusions which only contain a tiny fraction of the cell's total cytosol. Whereas the fraction of phosphorylated stathmin in these protrusions is significantly elevated compared to the rest of the cell, as indicated by our experiments, its total cellular fraction in line with the biochemical data (Daub, Gevaert et al. 2001) is likely to be minor. Importantly, the local difference in fractional phosphorylation of stathmin observed in the cell body and lamella is proposed to create a gradient of microtubule stabilizing activity which could guide

microtubules into the protrusions of migrating cells and selectively stabilize them there. In this thesis we did not experimentally address this possible consequence. However, stabilization of microtubules within lamella is already a well-known phenomenon which was termed “pioneering” (Waterman-Storer and Salmon 1997). Pioneer microtubules constitute a subset of cellular microtubules which have their ends located near the protruding edge of a migrating cell. Confronted with a strong retrograde actin flow, microtubules have to undergo net-growth to maintain their position near the leading edge, which constantly pushes forward. Indeed, these microtubules were shown to spend more time growing and undergo fewer catastrophes than polymers terminating in other regions of the cell. Pioneering is dependent on the activity of membrane located Rac1 GTPase. Recent studies propose Rac1-Pak1 mediated phosphorylation of stathmin to be at least in part responsible for this region selective behavior of microtubule growth (Wittmann and Waterman-Storer 2001; Wittmann, Bokoch et al. 2003; Wittmann, Bokoch et al. 2004).

Selective stabilization or “pioneering” of microtubules in migrating cells exemplifies how polarized growth helps to maintain the morphology of a dynamic microtubule array in interphase. Our study raises evidence for the idea that this process is mediated by the spatial regulation of diffusible microtubule regulatory activities. Taking stathmin/op18 as an example, it demonstrates how these activities structure the cytoplasm thereby providing possible guidance for growing microtubules.

B. Stathmin-tubulin interaction gradients in mitosis

We visualized gradients of stathmin-tubulin interaction around mitotic chromosomes and demonstrated that these gradients are dependent on stathmin phosphorylation. A lack of stathmin phosphorylation around chromosomes induces shorter spindles. These findings are consistent with previous studies which show that stathmin phosphorylation is mediated by an activity localized on mitotic chromatin (Andersen, Ashford et al. 1997; Budde, Kumagai et al. 2001) and that inhibition of stathmin phosphorylation seriously affects the mitotic spindle (Budde, Kumagai et al. 2001; Kuntziger, Gavet et al. 2001). Another study suggests that the phosphorylating activity is located on polymerized microtubules rather than on chromatin in mitotic *Xenopus* egg extracts (Kuntziger, Gavet et al. 2001). Our experiments neither confirm this assumption nor do they exclude it. However, in case of a major contribution of the microtubules we expected the highest amplitude of stathmin phosphorylation in the area around the spindle poles because the highest density of microtubules can be found there. Instead, we observed a unipolar gradient extending from the centre of the spindle where the chromosomes are located at metaphase.

Another steady-state gradient of the diffusible microtubule regulating activity RanGTP around mitotic chromosomes had previously been detected in *Xenopus* egg extracts also using ratiometric FRET probes (Kalab, Weis et al. 2002).

In contrast to the stathmin phosphorylation gradient, whose major role seems to be the localized stabilization of microtubules, the major physiological role of the RanGTP gradient is considered to be the de-novo nucleation of microtubules close to the chromosomes. However, the RanGTP- as well as the phospho-stathmin gradient are likely to be created by the same biochemical principle: In both cases, the production of a diffusible molecular species (RanGTP / phospho-stathmin) of specific

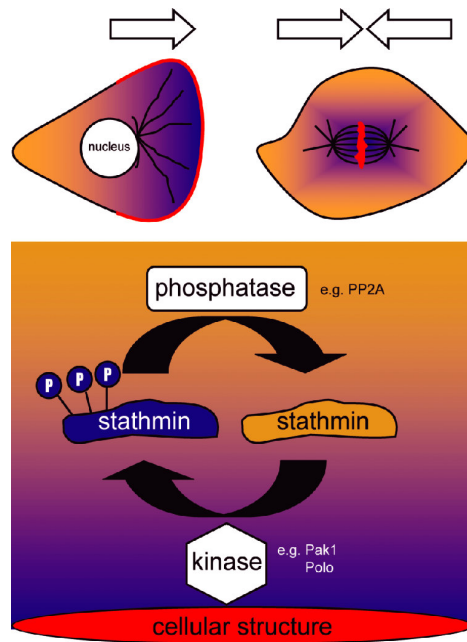
biological activity is correlated to the position of mitotic chromosomes due to the localization of an activating factor or enzymatic activity that is localized on these structures (RCC1 / Polokinese). Upon production, the species diffuse away from the structure creating a concentration gradient. Its extent is defined by a counteracting, homogeneously distributed cytosolic activity (RanGAP/ Protein phosphatase 2A) which removes the diffusing chromosome dependent activity from the cytosol again and thus can be theoretically estimated from the diffusion constant of stathmin and the total phosphatase activity in the cytoplasm (Brown and Kholodenko 1999). Although this is obviously a rough estimation it shows if gradients of the dimensions measured in this study are realistic under physiological conditions. We have approximated the diffusion constant of COPY to lie between 2-15 $\mu\text{m}^2/\text{s}$. The concentration of PP2A in *Xenopus* egg extracts was estimated to be 3-6 μM (Lin, Walter et al. 1998). This gives a total phosphatase activity at sub-saturating conditions of 0.3-0.7 s^{-1} given the K_m (10.8 μM) and k_{cat} (1.2 s^{-1}) values for PP2A (Price and Mumby 2000). The stathmin phosphorylation gradient will decay to 1/e of its initial intensity at 2-7 μm given these values and assuming a one-dimensional diffusion model (for details refer to Material and Methods). Importantly, this shows that phosphorylation gradients, like the ones we observed, are plausible within cellular dimensions assuming the counterplay of localized kinase and non-localized phosphatase activity as a creating principle.

In conclusion, the stathmin as well as the Ran system are likely to support a long distance connection between microtubules and chromosomes by creating a local environment of microtubule stabilizing or nucleating activity around mitotic DNA. This helps to maintain the spindle as a stable and at the same time highly dynamic, transient structure. Importantly, this long distance connection is not simply created by stereospecific interaction of proteins, but rather by a reaction diffusion system.

C. Conclusion

Besides *dynamic instability*, *search and capture* and *motor dependent reorganization*, *polarized growth* seems to be one of the major principles of microtubule selforganization into functional arrays.

In this thesis, we raise first evidence for the idea that polarized microtubule growth in cells is mediated by cytoplasmic microenvironments of differential microtubule stabilizing activity. Importantly, the maintenance of these microenvironments is dependent on the concentrations and the interplay of different molecular activities (see scheme below) and thus is a system feature. This study demonstrates how morphological information for the generation of a certain structure can be encoded by the physical and biochemical properties and interrelations of a set of system-components rather than by a single component's sequence.



Hypothetical scheme summarizing the factors necessary for the maintenance of a steady-state gradient of stathmin phosphorylation. Arrows indicate the polarization of the cytoskeleton.

V. Materials and Methods

A. Materials

A1. Chemicals

Common chemicals were of analytical grade and purchased from Sigma-Aldrich, Merck or Fluka. Special chemicals used for the study included:

5-(6)-carboxytetramethylrhodamine, succinimidyl ester (5(6)-TAMRA)	Molecular Probes
Okadaic Acid, Sodium Salt	Calbiochem
Phorbol 12-myristate 13-acetate (TPA, PMA)	Sigma-Aldrich
Activated p42 MAP kinase (Erk2)	New England Biolabs
cAMP dependent Protein kinase (catalytic subunit)	New England Biolabs
Chorionic gonadotropin (HCG)	Sigma-Aldrich

A2. Commonly used buffers, solutions and media

All solutions were prepared with double deionized water. Thereafter, solutions were sterile filtered or autoclaved and, unless indicated otherwise (in brackets), stored at room temperature.

3 x SDS sample buffer	150 mM Tris-HCl, pH 6.8 6 % [w/v] SDS
-----------------------	--

	30 % (v/v) glycerol 0.2 % (w/v) bromophenol blue 400 mM DTT (freshly added)
10 x Running buffer	0.25 M Tris 1.92 M glycine 1 % (w/v) SDS
10 % Resolving gel	375 mM Tris, pH 8.8 10 % (w/v) acrylamide/bisacrylamide 0.1% (w/v) SDS 0.1 % (w/v) APS 0.04 % (w/v) TEMED
3% Stacking gel	125 mM Tris, pH 6.8 3 % (w/v) acrylamide/bisacrylamide 0.1 % (w/v) SDS 0.1 % (w/v) APS 0.1 % (w/v) TEMED
10 x Transfer buffer	184 mM Tris 1.6 M Glycine
Ponceau S stain	0.25 % (w/v) Ponceau S 10 % (v/v) acetic acid
Coomassie blue stain	0.25 % (w/v) Coomassie Brilliant Blue R-250 10 % (v/v) acetic acid 12.5 % (v/v) isopropanol
Coomassie blue destaining solution	10 % (v/v) acetic acid 12.5 % (v/v) isopropanol
20 x Tris buffered saline (TBS)	3 M NaCl

	1 M Tris Adjusted to pH 7.5 with HCl
Stripping buffer	50 mM Tris 2 % SDS 100 mM β -mercaptoethanol adjusted to pH 6.8 with HCl
6 x DNA loading buffer	0.25 % bromophenol blue 0.25 % xylene cyanol FF 15 % Ficoll (type 400)
50 x TAE buffer	2 M Tris-acetate 50 mM EDTA, pH 8.0
LB medium (+ 4°C)	1 % (w/v) Bacto tryptone 0.5 % (w/v) Bacto yeast extract 170 mM NaCl adjusted to pH 7.6 with NaOH optional: 100 μ g / ml Ampicillin
BRB 80 buffer	80 mM potassium-pipes 1 mM MgCl ₂ 1 mM EGTA adjusted to pH 6.8 with HCl
MMR (1x) buffer	5 mM HEPES 100 mM NaCl 2 mM KCl 1 mM MgCl ₂ 2mM CaCl ₂ 0.1 mM EDTA adjusted to pH 7.8 with NaOH, auto-

	clave and store at RT
XB (1x) buffer	10 mM HEPES 100 mM KCl 0.1 mM CaCl ₂ 1mM MgCl ₂ 50 mM Sucrose adjust to pH 7.7 with KOH
CSF-XB	XB-buffer + 2 mM MgCl ₂ 5 mM EGTA adjust to pH 7.7 with KOH

A3. Instruments

QuantaMaster Spectrofluorometer	Photon Technology
UV/Visible Spectrophotometer Ultrospec 3000	Pharamcia Biotech
Ultracentrifuge Optima Max	Beckman Coulter
Centrifuge Avanti J-20 XP	Beckman Coulter
Centrifuge 5415C	Eppendorf
SDS-PAGE equipment	BioRad
Western Blot wet transfer unit	BioRad

Agarose gel electrophoresis equipment	EMBL mechanical workshop
Peltier Thermal Cycler PTC-200	MJ Research
Gene Pulser	BioRad
TCS SP2 Confocal microscope	Leica

A4. Kits

QIAquick PCR Purification Kit	Qiagen
QIAquick PCR Gel Extraction Kit	Qiagen
QIAprep Spin Mini Kit	Qiagen
HiSpeed Plasmid Maxi Kit	Qiagen

A5. Antibodies

anti-op18 (N-20) (sc-10899, NEB)	Goat polyclonal antibody raised against a peptide mapping at the amino terminus of stathmin of human origin.
anti-p-op18 (Ser 16) (sc-12948, NEB)	Goat polyclonal antibody raised against a peptide corresponding to a short amino acid sequence con-

	taining phosphorylated Ser-16 of p18 of human origin.
anti- α -tubulin (T-6199, Sigma-Aldrich)	Monoclonal anti- α -tubulin antibody produced in mouse. Clone DM1A.
anti-mouse-IgG-Cy5 (Amersham)	Cy5 tagged anti-mouse secondary antibody.
anti-goat-IgG-Fluor™ 633 (Molecular Probes)	Anti-goat antibody produced in rabbit and labeled with a dye with maximal emission at 633 nm.
anti-goat/sheep HRP (Sigma-Aldrich)	Monoclonal Anti-Goat/Sheep IgG-Peroxidase antibody produced in mouse. Clone GT-34.

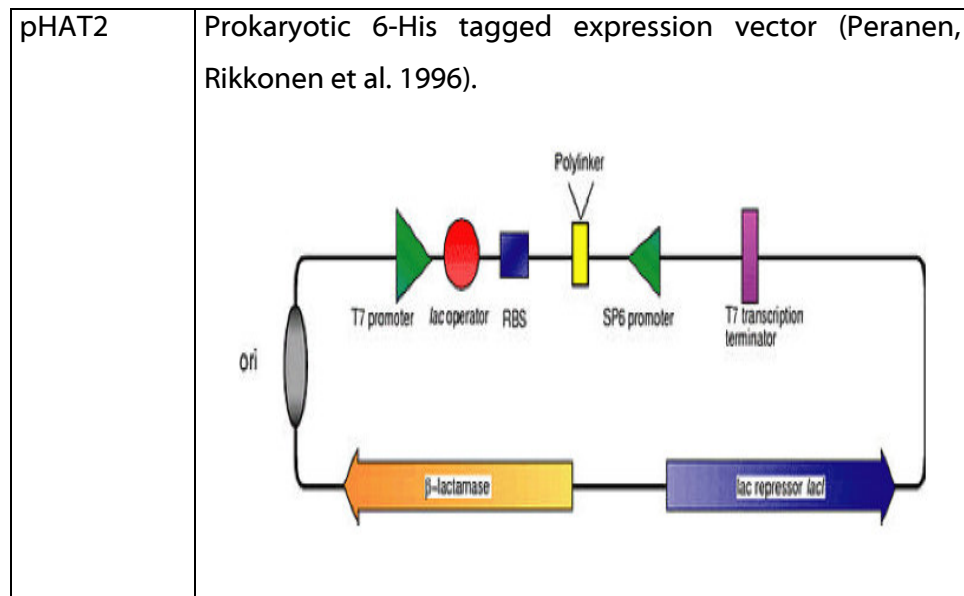
A6. Bacterial strains

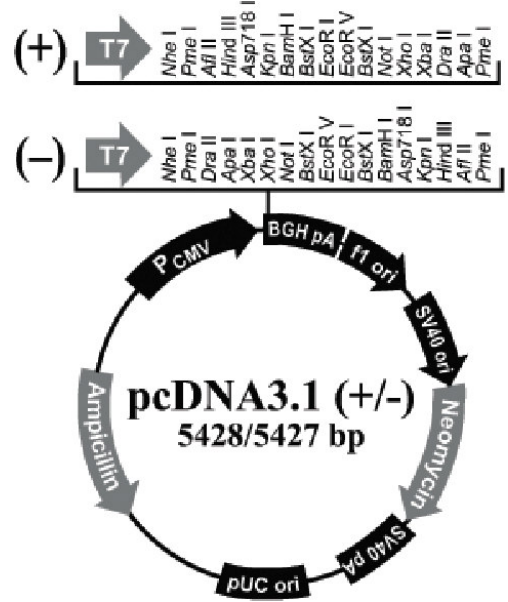
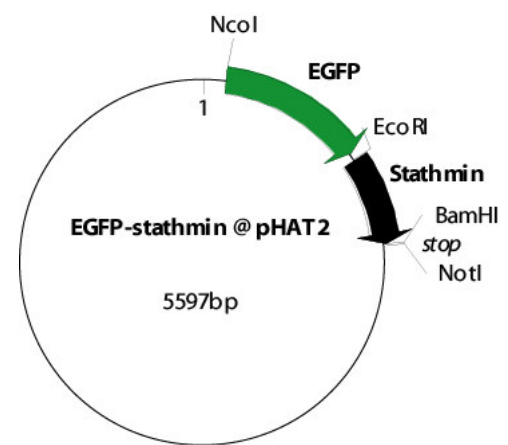
<i>E. coli</i> DH5 α	Bacterial strain regularly used for cloning experiments.
<i>E. coli</i> BL21	Bacterial strain used for high-level protein expression under IPTG-inducible promoters.

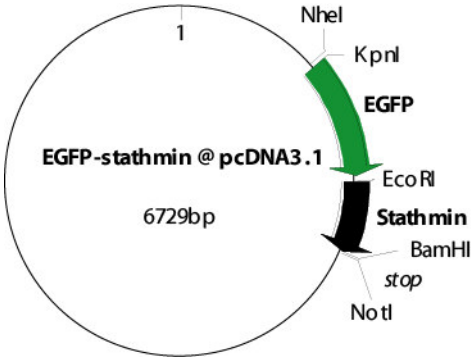
A7. Cell lines

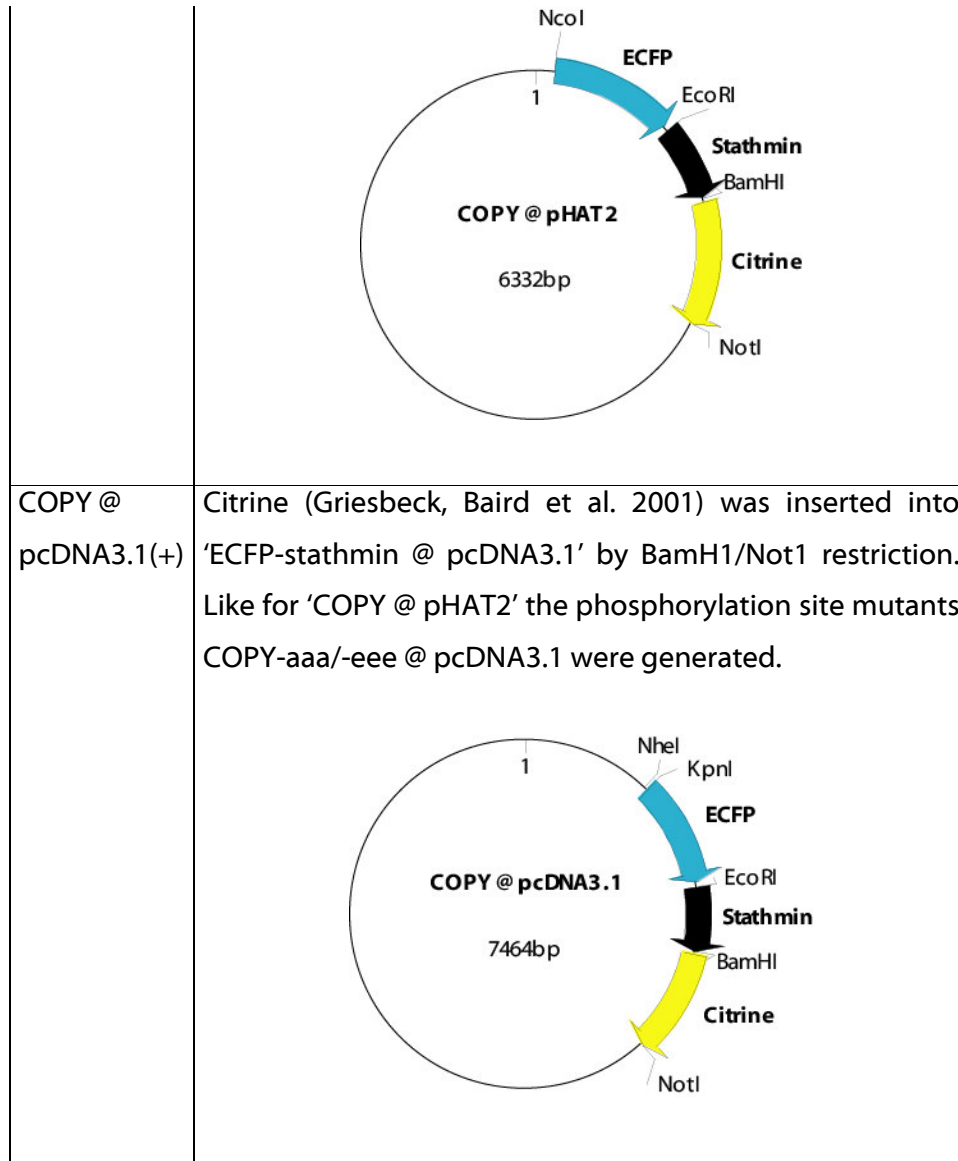
A6	Immortalized epithelial cell line from <i>Xenopus laevis</i> kidney. Cells are cultured in 70% L-15 Leibowitz medium supplemented with 15 % fetal calf serum (FCS) and 2 mM l-glutamine at 23 °C, 0 % CO ₂ . (ATCC number: CCL-102).
XL177	Cell line from <i>Xenopus laevis</i> (Miller and Daniel 1977). Cells are cultured in 70% L-15 Leibowitz medium supplemented with 15 % fetal calf serum (FCS) and 2 mM l-glutamine at 23 °C, 0 % CO ₂ . Cells have higher mitotic index than A6 cells.

A8. Plasmids



<p>pcDNA3.1(+)</p>	<p>Eukaryotic expression vector purchased from Invitrogen.</p> 
<p>Stathmin @ pMW172</p>	<p>6-His-<i>Xenopus</i> stathmin within a pMW172 vector (Way, Pope et al. 1990). For high-level expression in <i>Escherichia coli</i> the second residue of the stathmin-cDNAs is here mutated to Ala.</p>
<p>EGFP-stathmin @ pHAT2</p>	<p>Stathmin was amplified from 'stathmin @ pMW172' and flanked with an EcoRI and a BamHI restriction site by PCR. The PCR-product was inserted into EGFP-pHAT2 by EcoR1/Not1 digestion. A 6-His-sequence is present upstream the EGFP-stathmin sequence in the pHAT2 vector.</p> 

EGFP-stathmin @ pcDNA3.1(+)	<p>EGFP-stathmin was amplified by PCR from 'EGFP-stathmin @ pHAT2' and flanked with a Kpn1 and a Not1 restriction site by PCR. The PCR product was introduced into pcDNA3.1 by Kpn1/Not1 restriction.</p> 
ECFP-stathmin @ pHAT2	EGFP in 'EGFP-stathmin @ pHAT2' has been exchanged against ECFP by Nco1/BsrG1 restriction.
ECFP-stathmin @ pcDNA3.1(+)	EGFP in 'EGFP-stathmin @ pcDNA3.1' has been exchanged against ECFP by Nhe1/BsrG1 restriction.
COPY @ pHAT2	<p>Citrine (Griesbeck, Baird et al. 2001) was amplified by PCR from a source vector flanking it with a BamHI and a Not1 restriction site, respectively. The PCR product was inserted into 'ECFP-stathmin @ pHAT2' by BamHI/Not1 restriction. Ser-to-Ala and Ser-to-Glu phosphorylation site mutants of COPY (COPY-aaa/-eee) were generated by exchanging stathmin-wt against stathmin-aaa/-eee by EcoRI/BamHI restriction. Phosphorylation site mutants (Budde, Kumagai et al. 2001) were a kind gift of Dr. Rebecca Heald (Berkeley). Stathmin-aaa/-eee were amplified by PCR from the source vectors flanking the stathmin sequence with a EcoRI and a BamHI restriction site, respectively.</p>



B. Common DNA methods

B1. Polymerase chain reaction (PCR)

The PCR was used to generate DNA fragments for subcloning procedures. A typical 50 μ l reaction contained:

- 50 ng of template DNA
- 25 pmol forward oligonucleotide primer
- 25 pmol reverse oligonucleotide primer
- 250 μ M dNTP mixture
- 2.5 μ l DMSO
- 5 μ l 10 x Pfu buffer
- 1 μ l TurboPfu (Stratagene)

Sequences of interest were amplified using the following program:

- Initial denaturation: 95 °C for 1 min
- Denaturation : 95°C for 1 min
- Annealing : 60 °C for 1 min
- Elongation: 72°C for 1 min
- Final elongation: 72°C for 5 min

The denaturation, annealing and elongation steps were repeated for 30 times before the final elongation step. Quality and size of the amplified DNA fragments was analyzed on 1% agarose gels. Finally, PCR products were purified from the reaction mixture using the QIAquick PCR Purification Kit (Qiagen) following the manufacturer's instructions.

B2. DNA electrophoresis

Electrophoresis through agarose gels was used for separation, identification and purification of DNA fragments. DNA samples (200 ng for analytical or more for preparative electrophoresis) were mixed with DNA loading buffer and applied on 1 % agarose gels containing 0.5 µg/ml ethidium bromide. Gels submerged in 1x TAE buffer were run at high voltage (5-20 V/cm) and the separated EtBr-DNA complexes (1 EtBr molecule / 2.5 DNA bp) were visualized under UV light. Lengths of DNA fragments were estimated by their co-migration with fragments from a standard sample (GeneRuler™ 1kb DNA Ladder, Fermentas).

B3. DNA extraction from agarose gels

DNA fragments of interest were extracted from agarose gels using the QIAquick Gel Extraction Kit (Qiagen) following the manufacturer's instructions.

B4. Determination of DNA concentration and purity

DNA concentrations were determined by measuring the absorbance of diluted DNA samples at 260 nm in a spectrophotometer Ultrospec 3000 (Pharmacia Biotech). A solution containing dsDNA with an OD₂₆₀ of 1 has a concentration of approximately 50 µg dsDNA/ml. If samples contained insignificant amounts of phenol, DNA purity was estimated based on the OD₂₆₀:OD₂₈₀ ratio. Pure DNA solutions have an OD₂₆₀:OD₂₈₀ ratio of approximately 1.8.

B5. DNA digestion by restriction enzymes

DNA was digested with specific restriction enzymes for preparation of ligations during subcloning or for sequence analysis after subcloning procedures. A typical digestion reaction contained:

0.2 – 5 μg DNA-fragment or plasmid
0.1 $\mu\text{g}/\mu\text{l}$ bovine serum albumin (BSA)
1 U/mg DNA restriction enzyme
Restriction enzyme buffer in indicated dilution (usually 1:10)

The minimal reaction volume was 20 μl . Digestions were carried out for 1-2 hours at 37 °C. Vectors digested for a subsequent ligation were dephosphorylated using CIP alkaline phosphatase (New England Biolabs) to prevent vector self-ligation.

B6. DNA ligation

Cleaved and purified DNA inserts and vectors were ligated using T4 DNA ligase (New England Biolabs) in the corresponding ATP-containing ligation buffer. The total reaction volume was typically 10 μl . Because an appropriate molar ratio of insert to vector is important for obtaining an optimal number of “correct” ligation products, usually three reactions were set up containing equal amounts of vector and varying amounts of insert as well as two negative controls, one containing no insert and one containing no enzyme. After overnight ligation at 16°C, typically 7 μl of the ligation reaction was used to transform competent bacterial cells (DH5 α).

B7. Transformation of competent bacteria

Chemically competent *E.coli* DH5 α cells (50 μ l) were thawed on ice and incubated for 30 min with plasmid DNA on ice. Afterwards, the bacteria were heat-shocked for 45 s at 42°C in a waterbath and subsequently chilled for 10 min on ice. 1 ml of LB-medium was added and the suspension was incubated for 45 min at 37°C. The suspension was centrifuged for a few seconds in an Eppendorf centrifuge to pellet the bacteria. The supernatant was removed and the bacteria pellet resuspended in 100 μ l LB-medium. 50 μ l of this suspension was then plated on LB-agar-plates supplemented with an appropriate antibiotic (Ampicillin 50 μ g/ml). Colonies were grown for 20-24 h at 37°C.

B8. Lipid mediated transfection of eukaryotic cells

For cationic lipid mediated transfection with Lipofectamine Plus (Invitrogen), *Xenopus* A6 cells were seeded in six well dishes (Nunc) to reach a density of approximately 80% on the next day and then transfected according to the Lipofectamine Plus-Protocol. Briefly, 2 μ g/well pcDNA3.1(+) based expression plasmid was precomplexed with 6 μ g/well PlusTM reagent in 100 μ l/well serum-free Dulbecco's modified Eagle medium (DMEM) for 15 min at room temperature. Thereafter, 4 μ g/well LipofectamineTM in 100 μ l/well serum-free DMEM was added. This mixture was incubated for another 15 min at room temperature. In the meanwhile, the cells were washed two times with 2 ml serum-free DMEM per well and then layered with 0.8 ml/well serum-free medium. The plasmid / LipofectamineTM / PlusTM mixture was added to the cells and incubated for approximately 3.5 hours. Then, the transfection reaction was stopped by exchanging the serum-free transfection medium against L15-Leibowitz medium supplemented with 15 % fetal calf serum (FCS). Approximately 24 h after transfection, cells were replated on 15 mm-polylysine coated coverslips or, in case of live-cell experiments, on

Matek-dishes (Matek Corporation). They were grown another day allowing a total expression time of approximately 48 hours for the protein before microscopic analysis or fixation.

B9. Transfection of eukaryotic cells by electroporation

Xenopus XL177 cells were propagated like A6 cells, but transfected by electroporation as follows. Cells from one 70-80% confluent 90 mm Petri dish were collected, washed with 70% PBS, resuspended in 200 μ l 70% PBS with 20 μ g plasmid DNA. The mixture was incubated for 10 min on ice and then electroporated within 0.2 cm cuvettes (Gene Pulser™, Bio-rad) at 220 V, 200 Ω and 250 μ F. Subsequently, cells were plated on poly-L-lysine coated coverslips. Non-adherent (dead) cells were removed after approximately 8 hours by exchanging the medium (L15-Leibowitz, 15% FCS). Cells were grown for approximately 48 hours after transfection.

C. Common biochemical methods

C1. Preparation of *Xenopus* egg extracts

CSF-arrested *Xenopus* egg extracts were prepared according to Murray (Murray 1991).

Briefly, female *Xenopus laevis* frogs were injected with 0.25-0.5 ml of 20000 IU/ml (500-1000 units) of human chorionic gonadotropin (HCG, Sigma). Frogs were kept overnight in 1x MMR at 16-18°C for about 16 h. On the next morning the eggs were collected into glass beakers previously rinsed with dH₂O. Eggs of different quality were kept in separate batches.

Eggs were washed several times with 1x MMR to remove skin and other detritus. During this procedure activated eggs were removed.

The remaining eggs were incubated with dejelling solution (2% (w/v) cysteine, adjusted to pH 7.8 with NaOH) for 5-10 min until the eggs tightly packed together. Then the dejelling solution was removed and the eggs were washed two times with XB buffer. Again, activated or abnormal eggs were removed as much as possible. Eggs were washed two times with CSF-XB and finally kept in CSF-XB + Protease-inhibitors (100 x solution: 1 tablet EDTA complete™ in 0.5 ml H₂O).

Eggs were transferred with a cut Pasteur pipette to Beckman SW50 centrifuge tubes containing 0.5 ml CSF-XB + 5 µl protease inhibitors and 1 µl cytochalasin D (10 mg/ml in DMSO) and the liquid was removed from the top of the egg layer. The tubes were placed into adapter tubes and the eggs were packed by centrifugation at 800 rpm (200 x g) for 1 min followed by centrifugation at 1600 rpm (400 x g) for 30 s at 16°C in a table top centrifuge (Beckman). Again, all liquid was removed from the top of the egg layer. Eggs were then crushed by centrifugation at 4°C in a JS13.1 rotor at 10500 rpm (about 17,000xg) for 20 minutes.

The tubes were put on ice and the cytoplasmic layer was collected by piercing the tube with a syringe and 18-gauge needle from the side. 1:100 of protease inhibitor- and 1:500 of cytochalasin D stock solution was added to the extract. Mitotic activity of the extract was checked by taking 20 µl extract and adding 0.8 µl of sperm nuclei and 0.2 µl of R-tubulin. The mixture was incubated at 20°C for 30-60 min. Mitotic activity of the extract was judged by its ability to condense DNA and to form half-spindles.

C2. Rhodamine labeling of tubulin

A concentrated stock of pig-brain tubulin solution was thawed as quickly as possible making sure that it did not warm above 4°C. Per labeling reaction, 10 ml of 8 mg/ml tubulin in BRB80 buffer was prepared by dilution the concentrated tubulin stock. The diluted solution was kept on ice and its MgCl₂ concentration was adjusted to 3.5 mM using a 1 M MgCl₂ stock. Similarly, the GTP concentration was adjusted to 1 mM using a 100 mM

GTP stock. The mixture was incubated on ice for five minutes and subsequently transferred to 37°C. 5 ml of pre-warmed glycerol was added to promote polymerization and the solution was incubated 40 minutes at 37°C.

In a 70Ti tube (Beckman), polymerized tubulin was put on 9 ml warm (37°C) high pH cushion (0.1M HEPES / NaOH, 1 mM MgCl₂, 1 mM EGTA, 60% (v/v) glycerol, pH 8.6). Microtubules were pelleted at 40,000 rpm for 45 min at 35°C, using a 70Ti rotor (Beckman).

The supernatant above the cushion was aspirated and the supernatant/cushion interface was rinsed twice with warm labeling buffer (0.1M HEPES / NaOH, 1 mM MgCl₂, 1 mM EGTA, 40% (v/v) glycerol, pH 8.6). The cushion was aspirated and the pellet was resuspended in 1.9 ml warm labeling buffer using a cut-off pipette tip. The tubulin was kept at 37°C during the process of resuspension.

The succinimidyl ester-coupled fluorophore (5(6)-TAMRA dissolved in DMSO) was added to a final concentration of 5 mM (corresponding to a 10 - 20 fold excess over the tubulin concentration assuming that the polymerization efficiency had been 70 % (the final DMSO concentration should be 10 % or less)). The fluorophore was added in two steps: First only 2.5 mM, the second 2.5 mM after 20 min. The tubulin / dye mixture was kept at 37°C the entire time and vortexed gently every 5 min. From now on, the sample was kept covered with aluminium foil to protect it from light.

The labeling reaction was put on a pre-warmed 1.4 ml low pH cushion (60 % (v/v) glycerol in BRB80) in a tube for the TLA 100.4 rotor (Beckman), and centrifuged at 80,000 rpm for 20 min at 35°C.

After the spin, the supernatant above the cushion was aspirated and the supernatant / cushion interface rinsed twice with warm BRB80. Afterwards, the cushion was aspirated and the pellet was briefly washed with warm BRB80 and resuspended in 1 ml of ice-cold depolymerization buffer (50 mM K-Glutamate, 0.5 mM MgCl₂, pH 7.0). The pellet was resuspended and incubated for 30 min on ice.

Subsequently, the depolymerized tubulin was centrifuged in a 120.2 rotor (Beckman) at 80,000 rpm for 10 min at 2°C and the supernatant was

recovered. BRB80 was added to 1x final (from a 5x BRB80 stock solution). $MgCl_2$ concentration was adjusted to 4 mM using a 1 M stock, GTP concentration to 1 mM using a 100 mM stock. The mixture was incubated on ice for 3 min and subsequently warmed to 37°C for 2 min. 1:2 volume of glycerol was added, mixed well, and the mixture was incubated 30 min at 37°C for polymerization. The polymerization reaction was put on a pre-warmed 1.4 ml low pH cushion in a TLA 100.4 rotor tube (Beckman) and microtubules were pelleted at 80,000 rpm for 20 min at 37°C. Thereafter, the supernatant above the cushion was aspirated and the supernatant cushion interface was rinsed twice with warm BRB80. Then, the cushion was aspirated and the pellet was briefly rinsed twice with 1 ml warm BRB80. The pellet was resuspended in 0.2 ml of ice cold BRB80 using a cut-off pipette tip. The solution was incubated for 20 min on ice. Now, the depolymerized tubulin was centrifuged 10 min in a TLA 100 rotor (Beckman) at 80,000 rpm at 2°C. After the spin the supernatant was recovered.

The R-tubulin concentration and the labeling ratio were determined as follows: The labeled tubulin was diluted 1:100 in BRB80 and an absorbance spectrum from 260 nm to beyond the absorbance peak of the dye was measured. The tubulin concentration was calculated from its molar extinction coefficient at 280 nm of 115,000 $M^{-1}cm^{-1}$. Similarly, the concentration of the fluorophore was calculated from its molar extinction coefficient at the absorbance maximum (provided by the manufacturer).

C3. Expression and purification of recombinant stathmin

BL21 cells were transformed with GFP-stathmin, COPY-wt, -aaa, -eee cDNA within pHAT2. An overnight culture of the transformed bacteria was grown in LB-medium supplemented with 50 $\mu g/ml$ ampicillin. The next day, this culture was diluted 1:50 in LB-medium supplemented with ampicillin and incubated at 37°C in a shaker until the optical density of the culture at 600 nm (OD_{600}) reached a value of 0.5. Then, IPTG was

added to the culture to yield a final concentration of 0.5 mM. The culture was incubated at room temperature under constant shaking. The bacteria were pelleted and the pellet was frozen in liquid nitrogen.

The pellet of 500 ml bacteria was thawed on ice and re-suspended in 20 ml HEPES- buffer (25 mM HEPES, pH 7.5) supplemented with protease inhibitors (leupeptin, pepstatin, and aprotinin, 100 µg/µl). Cells were lysed by passing them twice through a French Press. The homogenized bacteria suspension was centrifuged for 30 min at 10,000 rpm at 4°C and the supernatant was incubated with 2 ml Talon resin (Talon™ IMAC Resin; CLONTECH) for 1 h at 4 °C. After incubation, the resin was put on a column with a filter inlet and the flow through was recovered. The resin was rinsed extensively until the flow-through was colorless. A cap was put on the tip of the column and 2 ml of 100 mM imidazole in HEPES-buffer was incubated with the resin for 10 min. First, two fractions of 1 ml were eluted, second 5 ml of 100 mM imidazole in HEPES-buffer was added at once and 1 ml fractions of the eluate were recovered. An aliquot of each fraction was analyzed by SDS-PAGE and Coomassie staining. The most pure and concentrated fractions were pooled and then loaded onto a desalting column (PD10, Amersham Biosciences) that had been equilibrated with BRB 80. The eluate was concentrated using a centrifugal filter device (Millipore) with an appropriate molecular mass cut-off. Thereafter, the protein concentration was determined by absorption at A_{280} using the theoretical absorption coefficient calculated by the Protean-software (DNASTAR).

C4. *In vitro* phosphorylation of recombinant stathmin

A reaction-mixture of 4 µM COPY-wt or GFP-stathmin in BRB80 pH 6.8 containing 9 mM MgCl₂, 25 mM ATP, 2800 units activated p42 MAP kinase (New England Biolabs), 17500 units cAMP dependent Protein kinase (catalytic subunit, New England Biolabs) was incubated for 4 h at 27°C. Phosphorylation of the protein at Ser16 was assayed using a phosphospecific antibody (sc-12948, 1:2000, Santa Cruz Biotechnology, Inc.).

Non-phosphorylated COPY was detected by reprobing the membrane with an antibody against the N-terminus of stathmin (sc-10899, 1:2000, Santa Cruz Biotechnology, Inc.). Westernblot signals were quantified by band density analysis using the ImageJ software (Version 1.30v; Wayne Rasband, NIH, USA).

C5. SDS-polyacrylamide gel electrophoresis (SDS-PAGE)

Analytical sodium dodecylsulfate polyacrylamide gel electrophoresis (SDS-PAGE) was carried out under conditions ensuring dissociation of protein complexes into their individual subunits. Briefly, samples were mixed with SDS sample buffer containing the SDS detergent and the reducing agent DTT and heated at 98 °C for 5 min. Applying a constant voltage of 80V for approximately 10 min, the samples passed a stacking gel of high porosity before they were concentrated in a very thin zone (or stack) on the surface of the resolving gel. Thereafter, negatively charged unfolded protein-SDS complexes were separated according to their molecular weight. Electrophoresis was carried out in running buffer at a constant voltage of 160 V until the desired resolution was reached as judged by the separation of a prestained molecular weight marker (BioRad). Separated proteins were stained with Coomassie blue solution or processed for Western Blotting analysis.

C6. Coomassie staining of gels

Gels were soaked under gentle rocking in Coomassie blue solution for 45 min at room temperature, washed with H₂O to remove the remaining dye and destained overnight in Coomassie blue destaining solution. Sufficiently destained gels were dried using a heated vacuum gel drying system (Zabona AG Basel).

C7. Western blotting

Proteins separated by SDS-PAGE were transferred to nitrocellulose membranes using a BioRad wet-transfer unit at 80 V for 120 min at 4°C following the manufacturer's instructions. Briefly, gels were overlaid with the membrane (0.45 μm , Schleicher & Schuell) and placed into sandwiches covered from each side by a sponge and three layers of Whatmann paper equilibrated in transfer buffer. The sandwiches were mounted into a wet-transfer unit (membrane facing positive electrode) together with an ice block and covered with transfer buffer. Once the transfer was completed, membranes were stained with Ponceau S solution to monitor transfer, destained in TBS and blocked in TBS containing 4 % low fat milk powder (Frema) or BSA for 1 h at room temperature or overnight at 4 °C. Following 1 h incubation with primary antibodies (diluted in blocking solution) and secondary antibodies conjugated to horseradish peroxidase (diluted in blocking solution), proteins were detected by the enhanced chemiluminescence kit (Roche Diagnostics). After incubation with primary and secondary antibodies membranes were washed 4 x 10 min in TBST (TBS, 1% Triton X100) and just before detection additionally in TBS for 10 minutes.

D. Fluorescence based methods

D1. Wavelength spectrum of COPY

A 2 μM solution of recombinant COPY-wt (BRB80 pH 6.8, RT) was excited with monochromatic light at the excitation maximum of CFP (430 nm) in a spectrofluorometer (QuantaMaster, Photon Technology, Inc.) and the emission spectrum (450-650 nm) before and after addition of 30 μM tubulin (pig-brain) was recorded. The spectra were corrected for dilution of the sample.

D2. Ratiometric analysis of COPY-tubulin interaction *in vitro*

Recombinant COPY proteins were measured in BRB80 pH 6.8 at RT in a quartz cuvette (Hellma Precision Cell, TypeN: 105.252-QS). CFP was excited with monochromatic light at a wavelength of 430 nm using a spectrofluorometer (QuantaMaster, Photon Technology, Inc.). CFP- and Citrin-peak-emissions were acquired simultaneously at 475 nm and 525 nm, respectively. Cycled pig-brain tubulin was added stepwise to the COPY solution and the ratio between the Citrin- and the CFP-emission was monitored for each step of tubulin addition. Fractional saturation (Y) of COPY was defined as

$$Y = \frac{R_0 - R}{R_0 - R_\infty}$$

with R being YFP/CFP-ratio at a certain total tubulin concentration, R_0 being the YFP/CFP-ratio before tubulin addition and R_∞ being the YFP/CFP-ratio at saturation of COPY (when no more change in ratio could be detected anymore). The concentration of free tubulin was calculated as

$$[T_{free}] = [T_{total}] - 2Y[S_{total}]$$

with $[T_{total}]$ and $[S_{total}]$ being the total amount of tubulin and stathmin present in the experimental system and Y the fractional saturation of COPY. The plot of $v = 2Y$ versus $[T_{free}]$ was fitted (SigmaPlot, SPSS Inc.) with

$$v = \frac{B_{max1}x}{K_{d1} + x} + \frac{B_{max2}x}{K_{d2} + x}$$

being a model assuming two independent sites for tubulin binding to stathmin. Each fit yielded $B_{max1} = B_{max2} \approx 1$.

D3. Ratiometric analysis of COPY-tubulin interaction in *Xenopus* egg extracts

6 μM recombinant COPY-wt was added to mitotic *Xenopus* egg extract. The extracts were incubated 30 min at 20°C with and without addition of 4 μM okadaic acid (sodium salt, Calbiochem). 12-bit confocal images of the extract were acquired with a SP2 confocal microscope (Leica) with a HCX PL APO 63.0x1.32 objective. CFP was excited with a 405 nm laser diode (50% power). CFP emission was sampled between 470 - 500 nm, YFP emission was sampled between 525 - 650 nm (4 line-averages, pinhole: 5.23 airy). Fluorescence images were smoothed (median filter) and the YFP/CFP-images were calculated.

D4. Determination of exogenous protein expression level in *Xenopus* cells

In order to determine the COPY expression level in transfected A6 cells, untransfected and transfected cells were stained with a primary stathmin-antibody (sc-10899, New England Biolabs) and a Fluor™ 633-labeled secondary antibody (Molecular Probes) and the average fluorescence intensity of both populations was compared.

D5. Ratiometric analysis of COPY-tubulin interaction in *Xenopus* cells

12-bit confocal images of COPY in *Xenopus* A6 cells were acquired with a SP2 confocal microscope (Leica) with a HCX PL APO 63.0x1.32 objective. CFP was excited with a 457.9 nm argon laserline (68% power). CFP emission was sampled between 470 - 500 nm, YFP emission was sampled between 525 - 610 nm (timelapse: 16 line averages, pinhole 3.5 airy; others: 8 line-averages, pinhole 3 airy). Cy5 emission was excited at 633 nm and

sampled between 650 nm to 800 nm. For mitotic XL177 cells, confocal z-Stacks were acquired and z-projected (average method) to yield the CFP- and YFP- intensity images (16 line-averages, pinhole: 1 airy). All image processing was done with ImageJ. The average background was measured in a square near the cell and subtracted globally. Images were smoothed (median filter) and thresholded. The ratio map of each cell was calculated by dividing the corrected fluorescence images (YFP/CFP). The ratio images were statistically analyzed as follows:

- a) *Spatial inhomogeneity assay (SIH)*: A square was drawn to fit the ratio image of the cell. 10 x 10 pixel squares were placed at the sites, where the diagonals hit the edges of the cell (r_1 - r_4) or each other (c) in the center. The mean ratio values in these squares were acquired. Relative ratiochanges ($(r_n - c) / c$) from the periphery to the inside were calculated and averaged for each cell. From these single cell SIH-values the average for the whole population was calculated (Results section, Figure 13).
- b) *Mitotic gradient analysis*: Mean ratios were measured within three circular areas around the center of the spindle (r_1 - r_3). The mean ratio in the rest of the cell (c) was set as base value. The relative difference (Δr) between the basal ratio value and the mean ratio of the three circular regions was calculated (Results section, Figure 18B).

D6. Acceptor photobleaching analysis of COPY-tubulin interaction in *Xenopus* cells

12-bit confocal images of COPY in *Xenopus* A6-cells were acquired with a SP2 confocal microscope (Leica) with a HCX PL APO 63.0x1.32 objective. The YFP signal was bleached (514 nm laserline) in rectangular quarters of the cells containing central as well as peripheral regions. CFP was excited with a 405 nm laser diode (33% power). CFP emission was sampled be-

tween 450 - 490 nm before and after bleaching (8 line-averages, pinhole: 1 airy). After background-correction and smoothing (median-filter), the prebleach-image was subtracted from the postbleach-image. The subtraction-image was divided (for all pixelvalues >0) by the postbleach-image to yield the FRET-efficiency-image. The mean FRET efficiency was measured in two arbitrary rectangular regions at the leading edge and in one region at the cell center. The average FRET difference was calculated for each cell and averaged for the whole population.

D7. Fluorescence recovery after photobleaching (FRAP)

FRAP experiments were performed at room temperature using a Zeiss LSM510 FCS confocal microscope with a 63x/1.4 Oil Plan-Apochromat objective and a 530-600 band pass filter. Within COPY-wt expressing XL177 cells, small circular regions of interest (ROIs) of YFP-fluorescence with a defined diameter (ranging from 3.86 μm – 5.46 μm) were bleached for 5 s using the 514 nm laserline. Fluorescence recovery in these regions was monitored by acquiring images every 140-170 ms. From the raw recovery curves (average ROI intensity versus time), the fractional recovery

$$FK(t) = \frac{FK(t) - FK(0)}{FK(\infty) - FK(0)}$$

was calculated, with $FK(0)$ being the average ROI intensity immediately after bleaching and $FK(\infty)$ being the intensity after full recovery when no significant change in intensity could be observed anymore. The fractional recovery curves ($t \rightarrow FK(t)$) were fitted with

$$f(t) = e^{-2\tau_D/t} \left[I_0 \frac{2\tau_D}{t} + I_1 \frac{2\tau_D}{t} \right]$$

as described by Soumpasis (Soumpasis 1983) to obtain τ_D with I_0 and I_1 being modified Bessel functions. The diffusion constant D derives from

$$\tau_D = \frac{\omega^2}{4D}$$

with ω being the radius of the bleaching beam.

E. Culture, drug treatment and immunostaining of cells

E1. Cell culture and freezing

Xenopus A6 and XL177 cells were grown in 70% L-15 Leibowitz medium (Sigma-Aldrich) supplemented with 15% fetal calf serum (FCS, Gibco) and 2 mM l-glutamine (Gibco) at 23°C without CO₂ on 10 cm tissue culture plates (Falcon). When the cells reached a density of approximately 80% confluence (every 3-4 days), they were split 1:3. Cells were grown up to 12 passages and then discarded. For freezing, cells from 2-3 10 cm cell culture dishes were harvested and resuspended in 1 ml cell culture medium supplemented with 10% DMSO. The cell suspension was slowly frozen in a 2-Propanol bath at 80°C using a Cryo-1°C-Freezing-Container (NALGENE™). For long-term storage, cell aliquots were kept in liquid nitrogen. Thawing of cells was performed quickly using a 37°C waterbath.

E2. Drug treatment of cells

Serum starved A6 cells were stimulated with serum-free L15-Leibowitz medium supplemented with 100 nM phorbol 12-myristate 13-acetate (TPA, Sigma) for 30 min at 23°C. Inhibition of phosphatases was per-

formed by simultaneous incubation with 6 μ M okadaic acid (sodium salt, Calbiochem). Thereafter, cells were immediately rinsed once with ice-cold PBS and then fixed with 4% paraformaldehyde in PBS.

E3. Fixation and immunostaining of cells

Cells were fixed with 4% paraformaldehyde / PBS for 15-25 min at room temperature and subsequently rinsed twice with quenching solution (0.1 M Tris-HCl, 0.1 M NaCl, pH 7.5). Thereafter, cells were washed three times for 5 min with PBS and incubated with primary antibody 30 – 60 min diluted in TPBS (1% (v/v) Triton X100 in PBS). Fluorescence labeling of the primary antibody was performed by incubating the cells with a fluorescently labeled secondary antibody for 30 min at room temperature. Coverslips were rinsed several times in PBS and mounted with Aqua Poly/Mount (Polysciences, Inc.). Fixed samples were stored at 4°C in darkness.

F. Estimation of gradient extent

The following differential equation describes the diffusion of a phosphorylated protein from a point source of kinase activity along one dimension. The phosphorylated species is removed by the activity of a homogeneously distributed phosphatase.

$$\frac{dP}{dt} = D \frac{d^2P}{x^2} - k_p P$$

With D being the diffusion constant for the phosphorylated species, x the distance from the kinase point source, P the concentration of the phosphorylated protein and k_p the first order rate constant of the phosphatase reaction.

The steady-state ($\frac{dP}{dt} = 0$) solution for this equation has the form

$$P(x) = P_0 e^{-x\sqrt{\frac{k_p}{D}}}$$

with P_0 being the initial concentration of the phosphorylated protein at the kinase point source. The value x at which P decreases to $1/e$ of its initial amplitude (P_0) is the decay length λ and defined as

$$\lambda = \frac{1}{\sqrt{\frac{k_p}{D}}}$$

The Michaelis Menten equation

$$v = \frac{v_{\max} P}{K_m + P} = \frac{v_{\max} \frac{P}{K_m}}{1 + \frac{P}{K_m}}$$

becomes

$$v = \frac{v_{\max} P}{K_m} = k_p P$$

assuming subsaturating conditions ($P \ll K_m$) for the phosphatase reaction. With

$$v_{\max} = k_{cat} E$$

follows

$$k_p = \frac{k_{cat}}{K_m} E$$

with E being the final concentration of the phosphatase. Realistic values for k_{cat} , K_m and E of PP2A were taken from literature (Lin, Walter et al. 1998; Price and Mumby 2000). We approximated with our FRAP-

experiments a value for D_{COPY} between 2-15 $\mu\text{m}^2/\text{s}$. From these data we calculated the theoretical decay length λ of the stathmin phosphorylation gradient (Discussion).

VI. References

- Andersen, S. S. (2000). "Spindle assembly and the art of regulating microtubule dynamics by MAPs and Stathmin/Op18." *Trends Cell Biol* **10**(7): 261-7.
- Andersen, S. S., A. J. Ashford, et al. (1997). "Mitotic chromatin regulates phosphorylation of Stathmin/Op18." *Nature* **389**(6651): 640-3.
- Bastiaens, P. I., I. V. Majoul, et al. (1996). "Imaging the intracellular trafficking and state of the AB5 quaternary structure of cholera toxin." *Embo J* **15**(16): 4246-53.
- Bastiaens, P. I. and A. Squire (1999). "Fluorescence lifetime imaging microscopy: spatial resolution of biochemical processes in the cell." *Trends Cell Biol* **9**(2): 48-52.
- Belmont, L. D. and T. J. Mitchison (1996). "Identification of a protein that interacts with tubulin dimers and increases the catastrophe rate of microtubules." *Cell* **84**(4): 623-31.
- Beretta, L., T. Dobransky, et al. (1993). "Multiple phosphorylation of stathmin. Identification of four sites phosphorylated in intact cells and in vitro by cyclic AMP-dependent protein kinase and p34cdc2." *J Biol Chem* **268**(27): 20076-84.
- Brattsand, G., G. Roos, et al. (1993). "Quantitative analysis of the expression and regulation of an activation-regulated phosphoprotein (oncoprotein 18) in normal and neoplastic cells." *Leukemia* **7**(4): 569-79.
- Brown, G. C. and B. N. Kholodenko (1999). "Spatial gradients of cellular phospho-proteins." *FEBS Lett* **457**(3): 452-4.
- Budde, P. P., A. Kumagai, et al. (2001). "Regulation of Op18 during spindle assembly in *Xenopus* egg extracts." *J Cell Biol* **153**(1): 149-58.
- Carazo-Salas, R. E., G. Guarguaglini, et al. (1999). "Generation of GTP-bound Ran by RCC1 is required for chromatin-induced mitotic spindle formation." *Nature* **400**(6740): 178-81.

- Carazo-Salas, R. E. and E. Karsenti (2003). "Long-range communication between chromatin and microtubules in *Xenopus* egg extracts." *Curr Biol* **13**(19): 1728-33.
- Cassimeris, L. (2002). "The oncoprotein 18/stathmin family of microtubule destabilizers." *Curr Opin Cell Biol* **14**(1): 18-24.
- Charbaut, E., P. A. Curmi, et al. (2001). "Stathmin family proteins display specific molecular and tubulin binding properties." *J Biol Chem* **276**(19): 16146-54.
- Chneiweiss, H., J. Cordier, et al. (1992). "Stathmin phosphorylation is regulated in striatal neurons by vasoactive intestinal peptide and monoamines via multiple intracellular pathways." *J Neurochem* **58**(1): 282-9.
- Curmi, P. A., S. S. Andersen, et al. (1997). "The stathmin/tubulin interaction in vitro." *J Biol Chem* **272**(40): 25029-36.
- Daub, H., K. Gevaert, et al. (2001). "Rac/Cdc42 and p65PAK regulate the microtubule-destabilizing protein stathmin through phosphorylation at serine 16." *J Biol Chem* **276**(3): 1677-80.
- Desai, A. and T. J. Mitchison (1997). "Microtubule polymerization dynamics." *Annu Rev Cell Dev Biol* **13**: 83-117.
- Di Paolo, G., B. Antonsson, et al. (1997). "Phosphorylation regulates the microtubule-destabilizing activity of stathmin and its interaction with tubulin." *FEBS Lett* **416**(2): 149-52.
- Dogterom, M., M. A. Felix, et al. (1996). "Influence of M-phase chromatin on the anisotropy of microtubule asters." *J Cell Biol* **133**(1): 125-40.
- Drouva, S. V., B. Poulin, et al. (1998). "Luteinizing hormone-releasing hormone-signal transduction and stathmin phosphorylation in the gonadotrope alphaT3-1 cell line." *Endocrinology* **139**(5): 2235-9.

- Förster, T. (1948). "Zwischenmolekulare Energiewanderung und Fluoreszenz." *Ann. Physik* **2**: 55-75.
- Gavet, O., S. Ozon, et al. (1998). "The stathmin phosphoprotein family: intracellular localization and effects on the microtubule network." *J Cell Sci* **111 (Pt 22)**: 3333-46.
- Gigant, B., P. A. Curmi, et al. (2000). "The 4 Å X-ray structure of a tubulin:stathmin-like domain complex." *Cell* **102(6)**: 809-16.
- Gordon, G. W., G. Berry, et al. (1998). "Quantitative fluorescence resonance energy transfer measurements using fluorescence microscopy." *Biophys J* **74(5)**: 2702-13.
- Goshima, G. and R. D. Vale (2003). "The roles of microtubule-based motor proteins in mitosis: comprehensive RNAi analysis in the *Drosophila* S2 cell line." *J Cell Biol* **162(6)**: 1003-16.
- Gradin, H. M., N. Larsson, et al. (1998). "Regulation of microtubule dynamics by extracellular signals: cAMP-dependent protein kinase switches off the activity of oncoprotein 18 in intact cells." *J Cell Biol* **140(1)**: 131-41.
- Griesbeck, O., G. S. Baird, et al. (2001). "Reducing the environmental sensitivity of yellow fluorescent protein. Mechanism and applications." *J Biol Chem* **276(31)**: 29188-94.
- Gruss, O. J., R. E. Carazo-Salas, et al. (2001). "Ran induces spindle assembly by reversing the inhibitory effect of importin alpha on TPX2 activity." *Cell* **104(1)**: 83-93.
- Gundersen, G. G. (2002). "Evolutionary conservation of microtubule-capture mechanisms." *Nat Rev Mol Cell Biol* **3(4)**: 296-304.
- Herman, B. (1989). "Resonance energy transfer microscopy." *Methods Cell Biol* **30**: 219-43.

- Holmfeldt, P., N. Larsson, et al. (2001). "The catastrophe-promoting activity of ectopic Op18/stathmin is required for disruption of mitotic spindles but not interphase microtubules." *Mol Biol Cell* **12**(1): 73-83.
- Horwitz, S. B., H. J. Shen, et al. (1997). "The microtubule-destabilizing activity of metablastin (p19) is controlled by phosphorylation." *J Biol Chem* **272**(13): 8129-32.
- Howell, B., N. Larsson, et al. (1999). "Dissociation of the tubulin-sequestering and microtubule catastrophe-promoting activities of oncoprotein 18/stathmin." *Mol Biol Cell* **10**(1): 105-18.
- Imamura, H., K. Takaishi, et al. (1998). "Rho and Rab small G proteins coordinately reorganize stress fibers and focal adhesions in MDCK cells." *Mol Biol Cell* **9**(9): 2561-75.
- Inoue, S. and E. D. Salmon (1995). "Force generation by microtubule assembly/disassembly in mitosis and related movements." *Mol Biol Cell* **6**(12): 1619-40.
- Jourdain, L., P. Curmi, et al. (1997). "Stathmin: a tubulin-sequestering protein which forms a ternary T2S complex with two tubulin molecules." *Biochemistry* **36**(36): 10817-21.
- Kalab, P., R. T. Pu, et al. (1999). "The ran GTPase regulates mitotic spindle assembly." *Curr Biol* **9**(9): 481-4.
- Kalab, P., K. Weis, et al. (2002). "Visualization of a Ran-GTP gradient in interphase and mitotic *Xenopus* egg extracts." *Science* **295**(5564): 2452-6.
- Karsenti, E., R. Bravo, et al. (1987). "Phosphorylation changes associated with the early cell cycle in *Xenopus* eggs." *Dev Biol* **119**(2): 442-53.
- Karsenti, E. and I. Vernos (2001). "The mitotic spindle: a self-made machine." *Science* **294**(5542): 543-7.

- Kirschner, M. and T. Mitchison (1986). "Beyond self-assembly: from microtubules to morphogenesis." *Cell* **45**(3): 329-42.
- Kline-Smith, S. L. and C. E. Walczak (2004). "Mitotic spindle assembly and chromosome segregation: refocusing on microtubule dynamics." *Mol Cell* **15**(3): 317-27.
- Kraynov, V. S., C. Chamberlain, et al. (2000). "Localized Rac activation dynamics visualized in living cells." *Science* **290**(5490): 333-7.
- Kuntziger, T., O. Gavet, et al. (2001). "Stathmin/Op18 phosphorylation is regulated by microtubule assembly." *Mol Biol Cell* **12**(2): 437-48.
- Kuntziger, T., O. Gavet, et al. (2001). "Differential effect of two stathmin/Op18 phosphorylation mutants on *Xenopus* embryo development." *J Biol Chem* **276**(25): 22979-84.
- Larsson, N., U. Marklund, et al. (1997). "Control of microtubule dynamics by oncoprotein 18: dissection of the regulatory role of multisite phosphorylation during mitosis." *Mol Cell Biol* **17**(9): 5530-9.
- Larsson, N., H. Melander, et al. (1995). "G2/M transition requires multisite phosphorylation of oncoprotein 18 by two distinct protein kinase systems." *J Biol Chem* **270**(23): 14175-83.
- Leighton, I. A., P. Curmi, et al. (1993). "The phosphorylation of stathmin by MAP kinase." *Mol Cell Biochem* **127-128**: 151-6.
- Lin, X. H., J. Walter, et al. (1998). "Protein phosphatase 2A is required for the initiation of chromosomal DNA replication." *Proc Natl Acad Sci U S A* **95**(25): 14693-8.
- Marklund, U., N. Larsson, et al. (1996). "Oncoprotein 18 is a phosphorylation-responsive regulator of microtubule dynamics." *Embo J* **15**(19): 5290-8.

- Maucuer, A., J. Moreau, et al. (1993). "Stathmin gene family: phylogenetic conservation and developmental regulation in *Xenopus*." *J Biol Chem* **268**(22): 16420-9.
- Melander Gradin, H., U. Marklund, et al. (1997). "Regulation of microtubule dynamics by Ca²⁺/calmodulin-dependent kinase IV/Gr-dependent phosphorylation of oncoprotein 18." *Mol Cell Biol* **17**(6): 3459-67.
- Miller, L. and J. C. Daniel (1977). "Comparison of in vivo and in vitro ribosomal RNA synthesis in nucleolar mutants of *Xenopus laevis*." *In Vitro* **13**(9): 557-63.
- Mimori-Kiyosue, Y. and S. Tsukita (2001). "Where is APC going?" *J Cell Biol* **154**(6): 1105-9.
- Mitchison, T. and M. Kirschner (1984). "Dynamic instability of microtubule growth." *Nature* **312**(5991): 237-42.
- Miyawaki, A. (2003). "Visualization of the spatial and temporal dynamics of intracellular signaling." *Dev Cell* **4**(3): 295-305.
- Murray, A. W. (1991). *Methods Cell Biol* **36**(36): 581-605.
- Nedelec, F., T. Surrey, et al. (2003). "Self-organisation and forces in the microtubule cytoskeleton." *Curr Opin Cell Biol* **15**(1): 118-24.
- Okamoto, I., Y. Kawano, et al. (1999). "Regulated CD44 cleavage under the control of protein kinase C, calcium influx, and the Rho family of small G proteins." *J Biol Chem* **274**(36): 25525-34.
- Ozon, S., A. Maucuer, et al. (1997). "The stathmin family -- molecular and biological characterization of novel mammalian proteins expressed in the nervous system." *Eur J Biochem* **248**(3): 794-806.
- Peranen, J., M. Rikkonen, et al. (1996). "T7 vectors with modified T7lac promoter for expression of proteins in *Escherichia coli*." *Anal Biochem* **236**(2): 371-3.

- Price, N. E. and M. C. Mumby (2000). "Effects of regulatory subunits on the kinetics of protein phosphatase 2A." *Biochemistry* **39**(37): 11312-8.
- Ravelli, R. B., B. Gigant, et al. (2004). "Insight into tubulin regulation from a complex with colchicine and a stathmin-like domain." *Nature* **428**(6979): 198-202.
- Redeker, V., S. Lachkar, et al. (2000). "Probing the native structure of stathmin and its interaction domains with tubulin. Combined use of limited proteolysis, size exclusion chromatography, and mass spectrometry." *J Biol Chem* **275**(10): 6841-9.
- Rowlands, D. C., A. Williams, et al. (1995). "Stathmin expression is a feature of proliferating cells of most, if not all, cell lineages." *Lab Invest* **72**(1): 100-13.
- Schatz, C. A., R. Santarella, et al. (2003). "Importin alpha-regulated nucleation of microtubules by TPX2." *Embo J* **22**(9): 2060-70.
- Segerman, B., N. Larsson, et al. (2000). "Mutational analysis of op18/stathmin-tubulin-interacting surfaces. Binding cooperativity controls tubulin GTP hydrolysis in the ternary complex." *J Biol Chem* **275**(46): 35759-66.
- Sells, M. A., A. Pfaff, et al. (2000). "Temporal and spatial distribution of activated Pak1 in fibroblasts." *J Cell Biol* **151**(7): 1449-58.
- Sobel, A. (1991). "Stathmin: a relay phosphoprotein for multiple signal transduction?" *Trends Biochem Sci* **16**(8): 301-5.
- Soumpasis, D. M. (1983). "Theoretical analysis of fluorescence photobleaching recovery experiments." *Biophys J* **41**(1): 95-7.
- Sprague, B. L., C. G. Pearson, et al. (2003). "Mechanisms of microtubule-based kinetochore positioning in the yeast metaphase spindle." *Biophys J* **84**(6): 3529-46.

- Steinmetz, M. O., R. A. Kammerer, et al. (2000). "Op18/stathmin caps a kinked protofilament-like tubulin tetramer." *Embo J* **19**(4): 572-80.
- Surrey, T., F. Nedelec, et al. (2001). "Physical properties determining self-organization of motors and microtubules." *Science* **292**(5519): 1167-71.
- Tournebize, R., S. S. Andersen, et al. (1997). "Distinct roles of PP1 and PP2A-like phosphatases in control of microtubule dynamics during mitosis." *Embo J* **16**(18): 5537-49.
- Walker, R. A., E. T. O'Brien, et al. (1988). "Dynamic instability of individual microtubules analyzed by video light microscopy: rate constants and transition frequencies." *J Cell Biol* **107**(4): 1437-48.
- Wallon, G., J. Rappsilber, et al. (2000). "Model for stathmin/OP18 binding to tubulin." *Embo J* **19**(2): 213-22.
- Waterman-Storer, C. M. and E. D. Salmon (1997). "Actomyosin-based retrograde flow of microtubules in the lamella of migrating epithelial cells influences microtubule dynamic instability and turnover and is associated with microtubule breakage and treadmilling." *J Cell Biol* **139**(2): 417-34.
- Way, M., B. Pope, et al. (1990). "Identification of a region in segment 1 of gelsolin critical for actin binding." *Embo J* **9**(12): 4103-9.
- Wittmann, T., G. M. Bokoch, et al. (2003). "Regulation of leading edge microtubule and actin dynamics downstream of Rac1." *J Cell Biol* **161**(5): 845-51.
- Wittmann, T., G. M. Bokoch, et al. (2004). "Regulation of microtubule destabilizing activity of Op18/stathmin downstream of Rac1." *J Biol Chem* **279**(7): 6196-203.
- Wittmann, T. and C. M. Waterman-Storer (2001). "Cell motility: can Rho GTPases and microtubules point the way?" *J Cell Sci* **114**(Pt 21): 3795-803.

Wollmann, R., E. Cytrynbaum, et al. (2004). A Ran GTP gradient can facilitate the Search-and-Capture of Chromosomes during Centrosome-directed Mitotic Spindle Assembly.

Wouters, F. S., P. J. Verveer, et al. (2001). "Imaging biochemistry inside cells." *Trends Cell Biol* **11**(5): 203-11.

Part of this thesis is published in the following article:

Niethammer, P., P. Bastiaens, et al. (2004). "Stathmin-tubulin interaction gradients in motile and mitotic cells." *Science* **303**(5665): 1862-6.

Abbreviations

aa	<i>amino acid</i>
APS	<i>ammonium persulfate</i>
ATP	<i>adenosine triphosphate</i>
BSA	<i>bovine serum albumine</i>
CFP	<i>cyan fluorescent protein</i>
COM	<i>center of mass</i>
COPY	<i>CFP-op18-YFP</i>
DMEM	<i>Dulbecco's modified eagle medium</i>
DMSO	<i>dimethylsulfoxide</i>
DNA	<i>deoxyribonucleic acid</i>
DTT	<i>dithiothreitol</i>
EDTA	<i>ethylenediaminetetraacetic acid</i>
EGF	<i>epidermal growth factor</i>
EGFP	<i>enhanced GFP</i>
Erk	<i>extracellular regulated kinase</i>
FCS	<i>fetal calf serum</i>
FRAP	<i>fluorescence recovery after photobleaching</i>
FRET	<i>fluorescence resonance energy transfer</i>
GAP	<i>GTPase activating protein</i>
GDP	<i>guanosine diphosphate</i>
GFP	<i>green fluorescent protein</i>
GTP	<i>guanosine triphosphate</i>
IgG	<i>immunoglobulin G</i>
IP	<i>immunoprecipitation</i>
IPTG	<i>isopropylthiogalactoside</i>
Kb	<i>kilobase</i>
kDa	<i>kilodalton</i>
LB	<i>Luria-Bertani medium</i>
MAP	<i>microtubule associated protein</i>
MAPK	<i>mitogen activated protein kinase</i>
OA	<i>okadaic acid</i>
OD	<i>optical density</i>
op18	<i>oncoprotein18</i>
PAGE	<i>polyacrylamide gel electrophoresis</i>
Pak	<i>p21 activated kinase</i>
PBS	<i>phosphate buffered saline</i>

PCR	<i>polymerase chain reaction</i>
PK	<i>protein kinase</i>
PP	<i>protein phosphatase</i>
ROI	<i>region of interest</i>
R-tubulin	<i>rhodamine tubulin</i>
S.E.M.	<i>standard error of mean</i>
SDS	<i>sodium dodecylsulfate</i>
SIH	<i>spatial inhomogeneity</i>
TAMRA	<i>tetramethyl rhodamine</i>
TBS	<i>Tris buffered saline</i>
TEMED	<i>N,N,N',N'.tetramethylethylenediamine</i>
TPA	<i>tetradecanoylphorbolacetat</i>
v/v	<i>volume/volume</i>
w/w	<i>weight/volume</i>
YFP	<i>yellow fluorescent protein</i>

Curriculum vitae

Personal details

Surname: Niethammer
 First name: Philipp Michael
 Title: Diploma Biochemist
 Date of birth: April 29, 1975
 Place of birth: Heilbronn, Germany
 Nationality: German
 Private address: Augustastrasse 17
 69126 Heidelberg, Germany
 Work address: EMBL Heidelberg
 Meyerhofstrasse 1
 69117 Heidelberg, Germany
 Email: niethamm@embl-heidelberg.de

Education

June 1994 *Abitur**
 Robert-Mayer-Gymnasium,
 Heilbronn, Germany
 Final mark (average): 1.1**
 July 1994 - July 1995 Military service
 October 1995 - Hamburg University
 December 2000 Study of Biochemistry/Molecular Biology
 Intermediate exam, mark: 1**
 Final exam, mark: ("Diplom"): 1**
 Title: Diploma biochemist
 (Februrary 2000 - Diploma thesis:
 December 2000) Center of Molecular Neurobiology (ZMNH),

* diploma from German secondary school qualifying for university admission
 ** mark: 1-6, 1 = top mark, 4 = pass

Hamburg
Supervisor: Prof. Dr. Melitta Schachner
Title: „Cosignaling of NCAM via the FGF-receptor and lipid rafts“
January 2001 - June 2001 Scientific co-worker in the laboratory of Prof. Dr. Melitta Schachner, ZMNH
July 2001 - November 2004 PhD thesis:
Participant in the *International PhD-Programme* at the European Molecular Biology Laboratory (EMBL), Heidelberg
Department of Cell Biology and Cell Biophysics
Supervisors:
Dr. Eric Karsenti, Dr. Philippe Bastiaens
Title: „ Stathmin tubulin interaction gradients in motile and mitotic cells“

First author publications

Cosignaling of NCAM via lipid rafts and the FGF receptor is required for neuritogenesis. *J Cell Biol.* 2002 Apr 29; 157(3): 521-32.

Stathmin-tubulin interaction gradients in motile and mitotic cells. *Science* 2004 Mar 19; 303(5665): 1862-6.

Course assistance

EMBL predoc course 2002, 2003, 2004

EMBO cell biology course 2003

Course participation

Physiology Course 2004, Marine Biological Laboratory, Woods Hole, Massachusetts

Acknowledgements

This study was carried out in the laboratories of Dr. Eric Karsenti and Dr. Philippe Bastiaens at the European Molecular Biology Laboratories in Heidelberg. I would like to thank both supervisors for giving me the opportunity for research in an open minded and creative scientific environment. Particularly, I would like to thank them for providing me a high degree of scientific freedom but also intensive advice whenever I needed it. In this respect, I should gratefully mention the long hours of discussion in Philippe's office which sharpened my recognition of the biophysical aspects of cell biology enormously.

Dr. Ian Mattaj (EMBL Heidelberg), a member of my thesis advisory committee, I would like to thank for his critical and productive comments.

PD Dr. Hartmut Quader (Hamburg University) and Prof. Dr. Eckhart Mandelkow (Max Planck Institute, Hamburg), I would like to thank for taking the effort and responsibility to be the referees of my PhD thesis. In this respect, I would like to thank PD Dr. Hartmut Quader for kindly helping me to organize my PhD application at Hamburg University.

I very much appreciate the friendly and supportive working atmosphere provided by the past and present members of Karsenti's, Bastiaens' and Vernos' labs; I am very pleased to have met them. In this respect I especially thank Tobias for keeping the table soccer challenge at EMBL alive (...with his fluky goals).

I would like to thank Uschi for always reminding me that there is a world beyond science and for giving me mental support whenever I needed it.

Finally, I would like to thank my mother, my father and my brother for being there and always encouraging me on my way.